BARIUM FLUORIDE (BaF_2) SCINTILLATION DETECTORS FOR FAST TIMING MEASUREMENTS IN PEBBLE-BED REACTOR DESIGN

A Thesis

by

XIAODONG TANG

Submitted to the Graduate and Professional School of
Texas A&M University
in partial fulfillment of the requirements for the degree of

MASTER OF SCIENCE

Chair of Committee,	Shikha Prasad
Committee Members,	Sunil S. Chirayath
	Lin Shao
	Sherry Yennello
Head of Department,	Michael Nastasi

December 2021

Major Subject: Nuclear Engineering

ABSTRACT

In this work, a barium fluoride (BaF_2) scintillation detector is investigated to determine if it can be used for fast measurement of deep burn fuel in advanced reactor designs. Pebble bed high-temperature gas-cooled reactors (HTGRs) have a multi-pass system of spherical fuel element circulation. Typically, the spherical fuel elements can be restricted from 55-hours to 100-hours of cooling time before recirculating or being used for another cycle through the system. In recent developments, a high purity germanium (HPGe) detector was utilized to detect gamma-rays where the pebble recirculates through a measuring site, and each pebble is measured for 10 seconds. However, a HPGe detector has a slow response time and therefore suffers from large dead time losses when exposed to the very high gamma-fields of a pebble (each pebble is ~ 1 kCi in radioactivity). A fast and efficient measurement system on the order of seconds is required for the pebble-bed's detection to remedy the problem. In this work, two objectives were investigated, and their results analyzed, i) BaF_2 energy response and resolution characterization for gamma-spectroscopy of a burned pebble by broadening energy peaks based on appropriate resolution ii) time response and resolution of the BaF_2 detector. To explore the energy resolution characterization for the gamma-spectroscopy, an optimal high voltage (HV) was first determined at 2.1 kV. Data was collected with CAEN's DT5730 digitizer using their CoMPASS software, the sampling rate of the digitizer being 250 MHz. The best energy resolution of BaF_2 was explored and found to be 16.62 ± 1.71%. The analog to digital converter (ADC) had 16,384 energy channels corresponding to the counts for the digitizer used in this research. All the energy bins were broadened to the Gaussian pulses and eventually summed up. A MATLAB script was created to perform the convolution numerically. The spectrum from Xenon-100 pebble, provided

by X-Energy was used. Secondly, to analyze the time resolution of the barium fluoride for fast measurement, a Python function was developed to process the collected data, fitted 200 pulses to the exponential curve, and the mean decay time was calculated as 0.99 and 648 ns for fast and slow components, respectively. Theoretically, the fast and slow time responses of the BaF_2 detector are 0.8 ns and 630 ns. These theoretical values were compared with the experimental data, and the error difference between them was calculated. In the future, the impact of this fast detection system on material balance and accounting will be explored by understanding how this system affects the inventory of ^{239}Pu and ^{235}U at a pebble bed reactor site.

ACKNOWLEDGEMENTS

I would like to thank my committee chair, Dr. Shikha Prasad, and my committee members, Dr. Sunil Chirayath, Dr. Lin Shao, for their support and expertise throughout this research. I would also like to thank Dr. Sherry Yennello and Dr. Alan Mclntosh from the Cyclotron Institute at Texas A&M University for lending us the BaF_2 scintillation detector and provide guidance and knowledge through the course of this research.

Thanks also go to my friends Yongchang Li and colleagues Benjamin Wellons and the department faculty Heather Haliburton Janke for making my time at Texas A&M University a great experience.

Finally, thanks to my mother and father for their encouragement.

CONTRIBUTORS AND FUNDING SOURCES

Contributors

This work was supervised by a thesis (or) dissertation committee consisting of Professor Shikha Prasad, Sunil S. Chirayath, and Lin Shao of the Department of Nuclear Engineering and Professor(s) Sherry Yennello of the Department of Chemistry.

The data analyzed for section VI.A.4 (Gamma-rays energy spectrum of the pebble bed were broadened by MATLAB) was provided by Professor Shikha Prasad from X-Energy. The data analyzed for section V.B.2 (Process the CoMPASS raw pulse data into a useful format for the further analysis) by using python code developed in Dr. Prasad's Neutron Sensing Laboratory by Xiaodong Tang and Benjamin Wellons.

All other work conducted for the thesis (or) dissertation was completed by the student independently.

Funding Sources

This work was also made possible in part by Texas A&M University, and Texas Engineering Experiment Station.

NOMENCLATURE

BaF_2	Barium Fluoride
PBMR	Pebble Bed Modular Reactors
HV	High Voltage
ADC	Analog To Digital Conversion
CFD	Constant fraction discriminator
LSB	Least Significant Bits
HTGRs	High-Temperature Gas-Cooled Reactors
HPGe	High Purity Germanium
FWHM	Full-Width Half Maximum
PET	Positron Emission Tomography
Cs	Cesium
Co	Cobalt
Pu	Plutonium
U	Uranium
MeV	Megaelectronvolt
KeV	Kiloelectronvolt
Nm	Nanometer
Ns	Nanosecond

TABLE OF CONTENTS

Page

LIST OF FIGURES

FIGURE Page

LIST OF TABLES

TABLE Page

I. INTRODUCTION

Scintillation crystals of barium fluoride (BaF_2) scintillation detectors are a good candidate for fast detection of gamma-rays. BaF_2 scintillators are characterized by sub-nanosecond timing and reasonable energy resolution. This means the BaF_2 can be utilized for the fast-timing measurement of deep burn fuel in advanced reactor designs. They are currently one of the fastest scintillation detectors due to their very fast light component and are employed in high-energy physics experiments. BaF_2 also has a relatively high-density crystal of 4.88 g/cm^3. It exhibits two decay components: a fast one with a decay time τ of 0.8 ns (the wavelength of maximum emission λ_{max} at 220 nm) and a slow one with a decay time τ of 630 ns (λ_{max} at 310 nm).[2] The fast component is responsible for the exceptionally good-time resolution properties of BaF_2. The slow component provides superior detection efficiency because 85% of gamma-rays are captured from the slow component. BaF_2's very fast light component allows the array to achieve reliable detection efficiency, reasonable energy resolution (around 15% FWHM), and a suitable timing resolution (sub-nanosecond).[2]

Objectives

There are two objectives of the research.

i. Explore the energy resolution characterization for gamma-spectroscopy, including high voltage determination, energy calibration, and the optimum energy resolution of the BaF_2 detector. Then implement the measured resolution onto the pebble bed spectrum by broadening the energy peaks.

ii. Find the time resolution of the fast response for a BaF_2 detector through measurements and fitting exponentials.

II. MOTIVATION

Pebble bed modular reactors (PBMR) may allow nuclear plants to support the goal of reducing global climate change in an energy-hungry world. These reactors are small, modular, inherently safe, use successfully demonstrated nuclear technology, and can be competitive with fossil fuels.

Pebble bed high-temperature gas-cooled reactors (HTGRs) have a multi-pass system of spherical fuel element circulation. They require a fast and efficient burn-up measurement system for the irradiated spherical fuel elements. Typically, the spherical fuel elements are restricted to a 55-hour cooling time before they can be recirculated or used for every cycle through the system.[4] Figure 1 is an existing measurement design for an HTGR where the pebble recirculates through a measuring site and emits gamma-rays to an HPGe.[4] (Figure 1). The HPGe detector only has a 10-second measurement time for each pebble. This is because when the detector goes to online processing, the pebbles fall at a rate of one pebble every 10 s. Existing HPGe detectors with microsecond long response times placed at pebble-beds are naturally disadvantageous for such fast measurement. HPGe not only has three orders of magnitude slower gamma-ray response times, but it also detects for a short period of time due to long-dead times and pileups. Therefore, a fast and efficient measurement system with a response time on the order of nanoseconds is required for pebble-bed detection to remedy the problem.

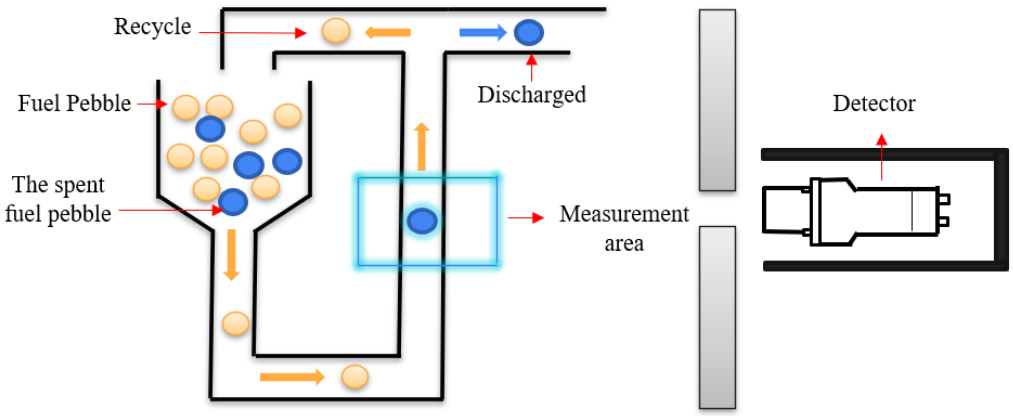

Figure 1. A measurement design for the HTGR where a pebble recirculates through a measuring site and emits gamma-rays to an HPGe.

The BaF_2 detector, with its extremely fast (sub-nanosecond) detection system, is known to be one of the fastest scintillation detectors. Because of this, it can perform high-efficiency gamma-spectroscopy on very high burn-up pebbles. The activity of one pebble after being burned in the reactor is one kCi (3.7×10^{13} Bq), and the modular-pebble-bed-reactor (MPBR) designs describe cores that contain a total of approximately 360,000 fuel pebbles.[5] When the BaF_2 detector was used for fast detection, it recorded an order of 1000 times more gamma-rays than the HPGe detector. Comparing the HPGe and BaF_2 further, the BaF_2 has a faster time response and no dead time for source-detector distances between 50 cm and 100 cm. It also has nanosecond fast charge multiplication and digitization systems. Because of these characteristics, BaF_2 was used to develop and design an extremely fast detection system capable of performing on-the-fly pulse analysis. However, there is one goal that researchers should be concerned about: the energy resolution of HPGe and BaF_2. Even though the BaF_2 has a faster response time and a much shorter dead time than the HPGe, the HPGe might offer better energy resolution and is a good instrument for unambiguous nuclide identification compared with the BaF_2 detector. The

HPGe detector also provides the advantage of resolving two closely located energy points and has the ability to detect a mixture of nuclear material. In this thesis, the researcher is going to measure and analyze the various measurement attributes related to the time and energy of a BaF_2 detector.

III. SCINTILLATION DETECTION MECHANISM

Scintillation counters are used to both measure and detect ionizing radiation by taking the excitation effect of incident radiation on the scintillator material and recording the resulting light pulses. A scintillation detector mainly consists of two parts. The first is the scintillation material, and the second is a photomultiplier. The scintillation material generates light photons in response to the energy deposited by the incident radiation. The sensitive photomultiplier tube (PMT) (or the photodiode) converts this scintillation light into electrical signal and electronics to process this signal.[21] Scintillation detection is widely used in radiation protection, assay of radioactive materials, and nuclear physics research. This is because they can be made inexpensively yet with good quantum efficiency and can measure the intensity and the energy of incident radiation.[21] The modern electronic scintillation counter was invented in 1944 by Sir Samuel Curran while working on the Manhattan Project at the University of California at Berkeley.[21] There was a requirement to measure the radiation from small quantities of uranium. To solve this, he used highly sensitive PMT tubes, which had been recently created by the Radio Corporation of America, to count the flashes of light from a scintillator which was subjected to radiation. This effort used previous research, including the discovery of radioactivity while working on phosphorescence of uranium salts by Antoine Heri Becquerel.[21] Previously, scintillation events had to be laboriously detected by the eye using a spinthariscope, which was a simple microscope to observe light flashes in a scintillator.[21]

Organic Scintillation Detector Mechanism

The process of fluorescence in organic scintillators comes from transitions in the energy level structure of a single molecule.[22] This allows it to be observed as a molecular species

regardless of its physical state of matter. Most organic scintillation materials bases on organic molecules containing certain symmetrical properties that allow for a π-electron structure.[22] Figure 2 shows the energy levels of molecules with this structure.

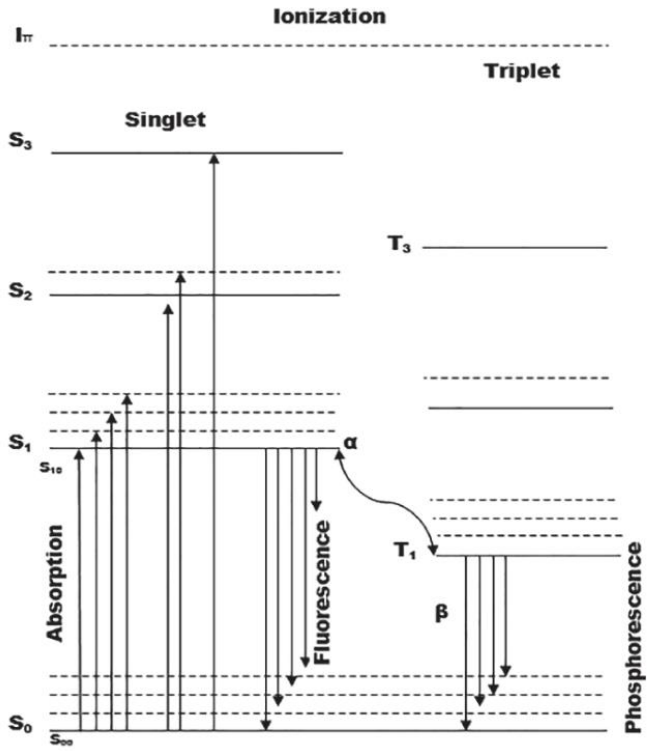

Figure 2. The energy level of an organic molecule with π-electron structure. Reprinted from **[***KNOLL, K. (2021). Radiation Detection & Measurement (3rd, 00) by Knoll, Glenn F [Hardcover (2000)] (3rd ed.). Wiley, Hardcover(2000).*]

In Figure 2, the absorption of energy by the molecules is [22] displayed as the arrows which point upward. For scintillators, these processes represent the absorption of kinetic energy from charged particles.[22] The higher singlet electronic states are excited quickly (on the order of picoseconds) de-excited to the S_1 electron state. The prompt flurorescence is emitted when transitions occur between the S_{10} state and a vibrational state of the ground state. [22] However, the lifetime of the first triplet state T_1 is characteristically much longer than that of the singlet state

S_1. Some excited singlet states may be converted into triplet states through a transition called intersystem crossing.[22] The lifetime of T_1 may be as much as 10^{-3} s and the radiation emitted in a de-excitation from T_1 to S_0 is therefore a delayed light emission characterized as phosphorescence.[22] Because T_1 lies below S_1, the wavelength of this phosphorescence spectrum will be longer than that for the fluorescence spectrum as shown in Table 1. Table 1 shows the fast and slow components of scintillation detectors and their relative characteristic.[2]

Table 1. The characteristics of the fast and slow components for scintillation detectors.[2]

	Fast component	Slow component
Response time (ns)	0.8	630
Type of light emit	Fluorescence	Phosphorescence
Wavelength (nm)	220	310

The number of such photons is proportional to the amount of energy deposited by the ionizing particle. The material will absorb and convert the energy of the incident particle into low energy photons. Consequently, the greater the energy of the incident radiation created the larger the number of photons.

Inorganic Scintillation Detector Mechanism

The scintillation mechanism depends on the crystal lattice structure, so there are two types of scintillators commonly used, organic scintillators and inorganic scintillators. Both NaI and BaF_2 are inorganic scintillation detectors. For such scintillators, the valence band is able to bind electrons at lattice sites, and the conduction band represents electrons with sufficient energy

to jump from the valence band to the conduction band.[22] There is an intermediate band called the *forbidden band* in which electrons can never be found in the pure crystal.[22] The energy absorption occurs when an electron jumps from the valence band to the conduction band leaving a hole in the valence band.[22] When the electron jumps back to the valence band in the pure crystal, photon emission is an inefficient process. The photon emitted by the typical gap width is too high to lie in the visible range.[22]

Small amounts of impurities are added to the crystal structure to increase the probability of visible photon emission during the de-excitation process.[22] These impurities are referred to as activators. Activators create special sites in the lattice at which the bandgap structure, also known as the energy structure, is modified.[22] This modification to the energy structure occurs only at the activator, not for the overall crystal structure.[22] (Figure 3)

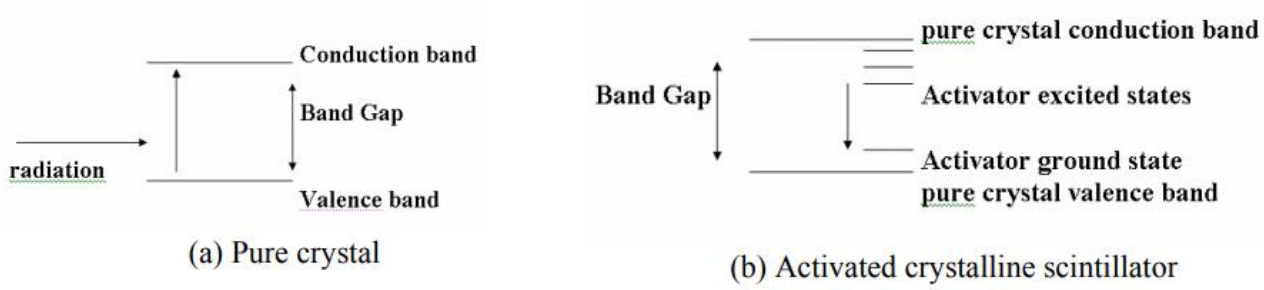

Figure 3. Energy band structure of an inorganic scintillator. Reprinted from **[***KNOLL, K. (2021). Radiation Detection & Measurement (3rd, 00) by Knoll, Glenn F [Hardcover (2000)] (3rd ed.). Wiley, Hardcover(2000).*]

The energy structure will be modified at the activator sites within the sample. Inside what would be the forbidden band in the pure crystal, energy states are created. This allows the electrons to de-excite through the levels going back to the valence band. Consequently, the

energy levels created by the activator's presence within the crystal are narrower than in the pure crystal and emission the visible photons.[22]

When the incident gamma-rays interact with the medium, the energy is absorbed and converted to the energetic electron through the photoelectric effect, Compton scattering, and pair production. These electrons create large numbers of electron-pulse pairs as they pass through the crystal. The positive holes will quickly move to an activator site, where the site is then ionized.[22] These sites are ionized because the ionization energy of the activator is less than that of a typical lattice site.[22] Electrons that are elevated to the conduction band are free to travel throughout the crystal until they finally encounter an ionized activation site.[22] The electron will fall into the site and create a neutral impurity with its own excited states.[22] Basically, the excited configuration will transition to a ground state. This de-excitation occurs very quickly and will likely produce a photon through emission. The activators are chosen such that the photons emitted will be in the visible spectrum of light.[22] There are also instances where an electron arriving at an impurity site creates an excited configuration which cannot transition to a ground state.[22] These instances then require an additional increment of energy raising them to a higher state, from which de-excitation to the ground state is finally possible.[22] One source of this extra energy is thermal excitation, and the resulting component of light from it is called phosphorescence.[2]

After scintillation light is produced, a portion of these low-energy photons arrives at the photocathode of an attached photomultiplier tube (PMT). The photocathode material, as in Figure 4, is placed between the scintillation crystal and the PMT. Low energy scintillation photons are focused on the photocathode, which results in a photoelectric effect and the emission

of photoelectrons or primary photoelectrons. These primary photoelectrons enter the PMT and multiply by a million times or more.[23] The purpose of the PMT is simply to provide an efficient collection geometry that accelerates electrons by a high-voltage field and greatly increases their number through an electron-by-electron multiplier. A photoelectron is electrostatically accelerated and focused by the electric potential causing it to hit the first dynode of the tube with a high kinetic energy. This primary electron's impact on the dynode then releases a number of secondary electrons. Each dynode after that releases even more electrons, creating a current amplifying effect at each dynode. Every stage is at a higher potential than the previous, providing an accelerating field. The resultant output signal at the anode is in the form of a measurement pulse for each group of photons that arrive at the photocathode and are passed to the processing electronics. The resulting pulse carries information about the energy of the original incident radiation on the scintillator. This is possible because when the photocathode induces a photoelectric effect, the binding energy of the electrons is relatively small, 13.6 eV, so the electrons can retain a large portion of the initial kinetic energy. This retained energy is proportional to the amount of energy the incident gamma-ray disposted. Figure 4 shows the completed scintillation detector mechanism.

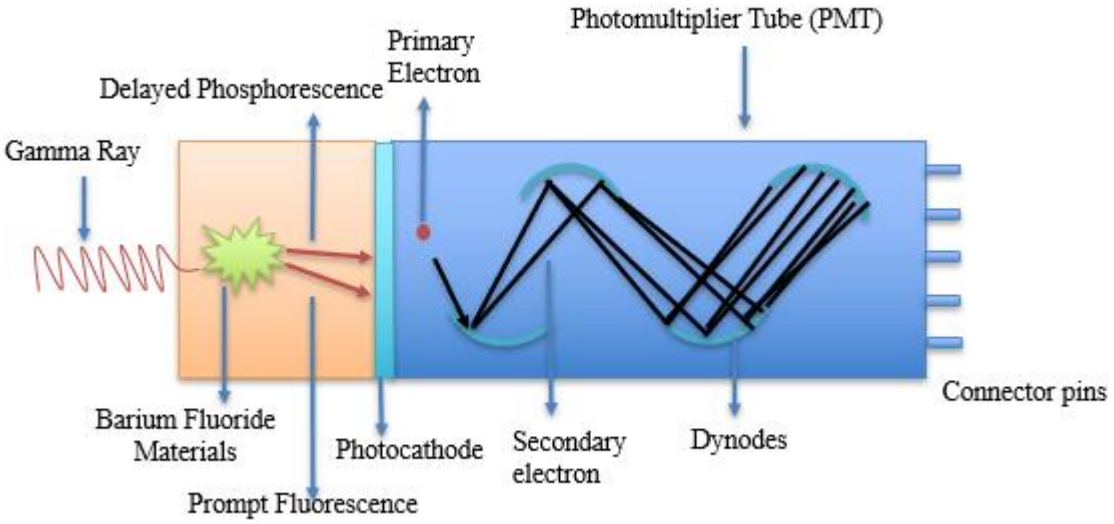

Figure 4. The scintillation detector mechanism**.**

Gamma-Ray Interaction Mechanism

A gamma-ray(γ) is a type of penetrating electromagnetic radiation (ER) produced by the radioactive decay of atomic nuclei. Gamma-rays were first discovered by Paul Villard in 1900 while studying radiation emitted by radium. In 1903, “Gamma Rays” were named by Ernest Rutherford based on their relatively strong penetration of matter.[24] . A gamma ray were defined as a component of radiation from uranum and radium which has a much higher penetrability than both alpha and beta particles. It is the shortest wavelength electromagnetic wave and so imparts the highest photon energy. [24]

There are many interaction mechanisms known for gamma rays. However, only three major types play a significant role in radiation measurement: photoelectric absorption, Compton scattering, and pair production. Photoelectric absorption predominates for low-energy gamma rays (up to several hundred keV), pair production predominates for high-energy gamma rays

(above 5-10 MeV), and Compton scattering is the most probable process over the range of energies between these extremes.[24]

Photoelectric Effect

As shown in Figure 5, a photon undergoes an interaction with an absorbing atom in which the photon completely disappears in the photoelectric absorption process. Assuming there is a piece of metal, and the electron is bound to the metal because it is attracted to positive charges in the nucleus. When the light is shining on the metal, an energetic photoelectron can be ejected from one of the inner shells of the atom. This interaction is with the atom as a whole and cannot take place with free electrons. For gamma rays of sufficient energy, the most probable origin of the photoelectron is the most tightly bound or K shell (13.6 eV) of the atom. The photoelectron appears with energy given by Eq (1).

$$E_e = hv - E_b \qquad Eq\ (1)$$

Where:

$E_{b:}$ represents the binding energy (13.6 eV) of the photoelectron in its original shell.

Hv: represented the energy of the incident photon energy.

Thus, for gamma-ray energies of more than a few hundred keV, the photoelectron carries off the majority of the original photon energy. Filling of the inner shell vacancy can produce fluorescence radiation, or x-ray photon(s).

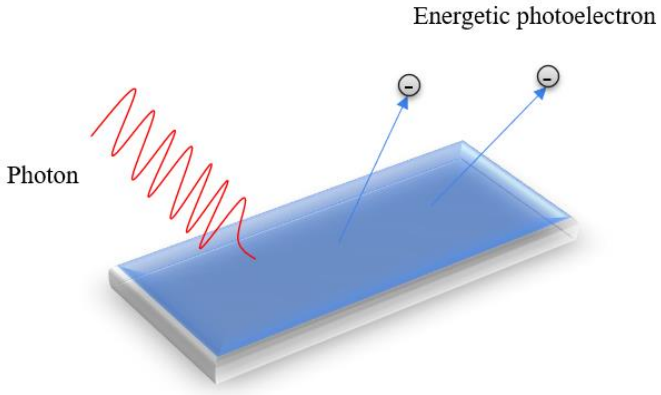

Figure 5. The photoelectric effect mechanism.

Compton Scattering

The photoelectric effect is when the gamma-ray loses all its energy in one interaction, and an inner shell vacancy produces fluorescence radiation. The process of Compton scattering on the other hand is when the incident gamma-ray (hν) interacts with an outer shell electron at rest in the target through an angle Θ with respect to its original direction.[28] The original gamma-ray transfers a portion of its energy to the electron which is called a recoil electron, and scatters lower energy photons (hν'). Compton scattering was discovered by Arthur H. Compton in 1922. Then he received the Nobel Prize in 1927 after he reported his theoretical explanation and experiment result. Figure 6 showed a schematic of Compton Scattering.[28]

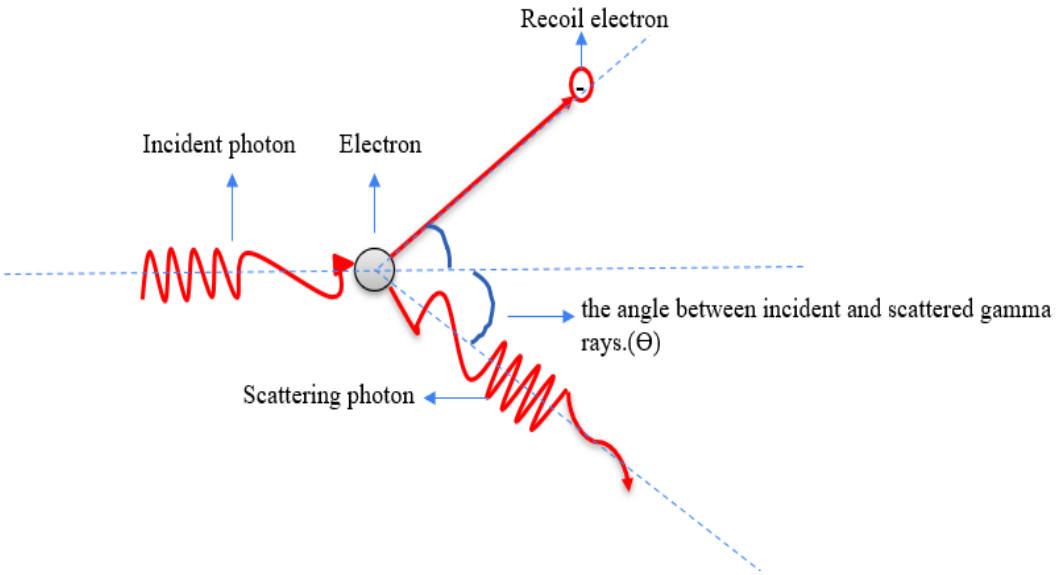

Figure 6. A schematic of Compton Scattering.

As compared with the photoelectric effect happening in the inner shell, the Compton scattering interaction involves the outer shell. The electrons are not tightly bound in the scattering atom, so their binding energy is very small (a few eV) compared with the incident gamma-ray. This means their binding energy can be ignored in the calculation. See Eq 2

$$E_e = E_\gamma - E'_\gamma \qquad Eq(2)$$

Where:

E_e= energy of recoil electron (Unit: keV)

E_γ= energy of the incident gamma ray (Unit: keV)

E'_γ= energy of the scattered photon. (Unit: keV)

To determine the amount of energy transferred to the recoil electron and scattered by the gamma-ray at different angles, Eq 3. expresses the relative energy of scattered gamma rays during the interaction.

$$E'_\gamma = \frac{E_\gamma}{1 + \frac{E_\gamma}{m_o c^2}(1 - cos\Theta)} \qquad Eq(3)$$

Where:

$m_o c^2$ = the rest mass energy of the electron (511 keV)

Θ = the angle between incident and scattered gamma rays.

E_γ= energy of the incident gamma-ray (Unit: keV)

E'_γ = energy of the scattered photon. (Unit: keV)

In table 2, when the scattered angle is 0°, the energy of the scattered photon is only slightly less than that of the incident gamma-ray and so the scattered electron can take only very little energy away from the interaction.[28] Oppositely, when the scattered angle is 180°, the energy is minimum for a head-on collision where the gamma-ray is scattered 180°, and the electron moves forward in the direction of the incident gamma-ray. The range of energy given to the scattered electrons can go from nearly zero to the maximum.[28]

Table 2. The minimum and maximum values of scattered photons and recoil electrons are determined.

Scattered angle of the photon (^{0})	E'_γ	E_e
0	E_γ	0
180	$\frac{E_\gamma}{1 + \frac{2E_\gamma}{m_o c^2}}$	$E_\gamma - \frac{E_\gamma}{1 + \frac{2E_\gamma}{m_o c^2}}$

Pair Production

The process of pair production occurs when a gamma-ray has sufficient energy of at least 1.022 MeV. The incident gamma-ray photon disappears and creates an electron and positron pair. The 1.022 MeV is twice the rest mass energy of an electron, and the incident gamma-ray must exceed it. Figure 7 shows a schematic of pair production.[26]

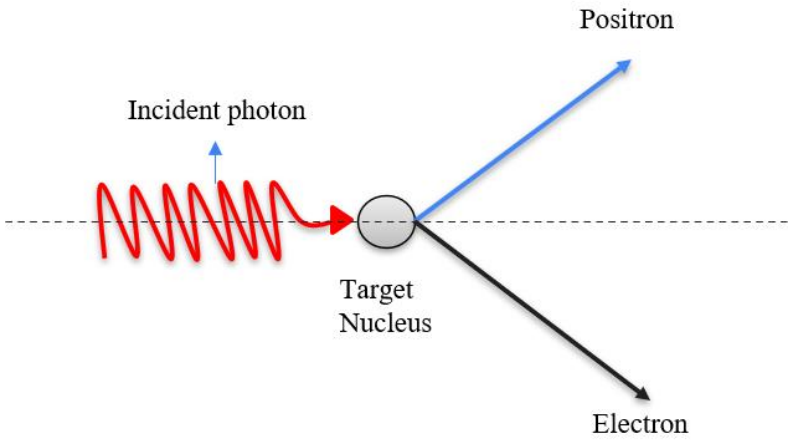

Figure 7. A schematic of pair production.

The annihilation phenomenon happens after the electron and position are rapidly slow in the medium, and the positron combines with an electron.[26] Two annihilation photons with energy of 0.511 MeV are normally produced as secondary products of the interaction. Figure 8 shows the schematic of the annihilation process. [26]

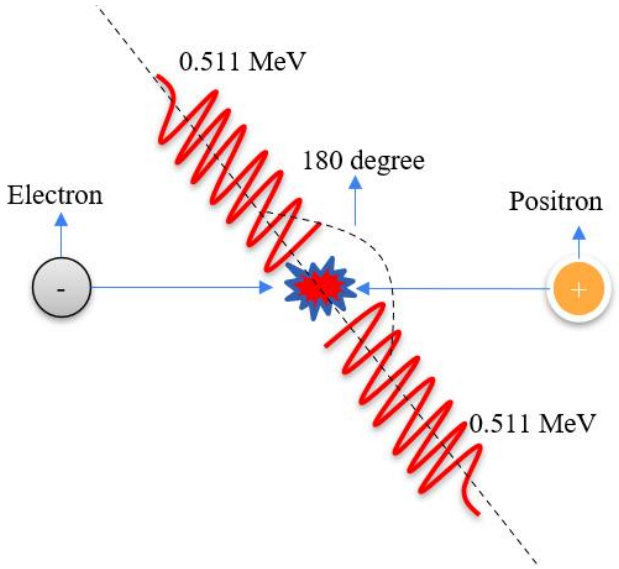

Figure 8. A schematic of annihilation process.

Scintillation Spectra (Photopeak)

In this research, gamma rays from ^{137}Cs and ^{60}Co sources are used as the source of photons that are scattered. Each photon has an energy of 0.662 MeV, 1.173 MeV, and 1.332 MeV when incident of the target. Based on the principle of the photoelectric effect, all the gamma rays are absorbed. If a ^{137}Cs source is placed near a scintillation detector, ideally, a single photopeak is shown in the gamma-ray spectrum as in Figure 9. However, all gamma-rays of the same energy do not produce the same exact number of visible photons in the scintillator. Because of this and the nature of counting statistics, the scintillation photons do not produce the same exact same number of photoelectrons from the photocathode of the PMT for the same amount of energy deposition in the scintillation crystal. Therefore, the distribution of the actual photopeak is a Gaussian distribution.[29]

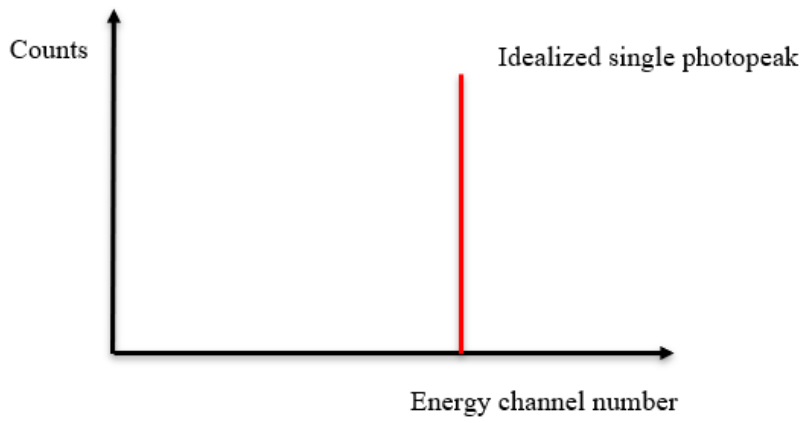

Figure 9. Idealized picture of a single photopeak caused by the photoelectric effect.

Scintillation Spectra (Compton Continuum)

In Compton scattering, when a gamma-ray interacts with the crystal, only a portion of the original energy is left with the electron and the energy of the scattered photon is less than the original photon energy.[29] The energy of the recoil electron is given in Eq. 2. This results in a smaller output of light, compared to previously discussed photoelectric absorption, when a gamma ray is completely absorbed by the crystal.[29] In a Compton scatter, the electron receives maximum energy at the scattered gamma-ray angle $\Theta = 180^{o}$, which corresponds to the Compton edge on a gamma-ray spectrum.[29] When the $\Theta=0^{o}$, there is no energy transfer. The processing of the Compton scattering differs as a function of angle, so the distribution of the Compton event of energy is less than the full 180° Compton edge. Figure 10 shows the photoelectric and Compton effect in the idealized gamma-ray spectrum.

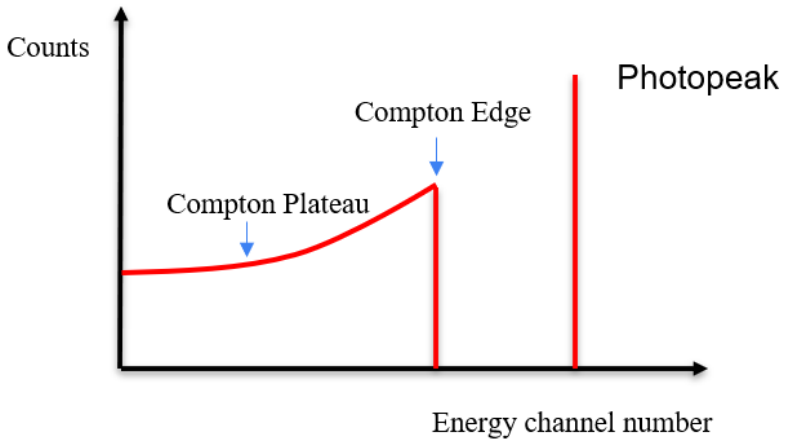

Figure 10. Idealized picture of the gamma-ray spectrum showing photopeak and Compton plateau.[29]

IV. LITERATURE REVIEW

Background and Past Work

BaF_2 detectors are currently the fastest known scintillators. They have an emission component with a sub-nanosecond decay time that results in very fast timing. This fast timing is necessary for positron lifetime studies, time-of-flight measurements, positron-emission-tomography (PET), and high-energy or nuclear physics applications.[2] By using special electronics, time resolution of around 200 picoseconds are possible with the use of very fast photomultiplier tubes and data acquisition systems.[2] BaF_2 detectors have several scintillation emissions bands, the fastest light emitted in the UV bands is centered between 195 and 220 nm.[2] They also have a relatively high-density crystal of 4.88 g/cm^3 and exhibit two decay components: a very fast one with a decay time τ of 0.6 ns (the wavelength of maximum emission λ_{max} at 220 nm) and a slow one with a decay time τ of 620 ns (λ_{max} at 310 nm).[3] The fast component is responsible for the exceptional time resolution properties of BaF_2. The slow component provides a good detection efficiency because 85% of gamma-rays are collected from the slow component.[2] To detect such fast scintillation light, it is necessary to use a photomultiplier tube with a good time resolution. Furthermore, the optical coupling compound must have excellent transparency for UV light.[2] The most common ones used are silicone oils or compounds. The use of a large scintillation crystal is possible because the self-absorption material is very low. The majority of scintillation light is produced by ionizing radiation interacting with the crystal by either pair production, photoelectric effect, or Compton scattering. The electrons from this interaction de-excite and in return emit photons in the UV range. Some de-excite quickly and others slowly based on the ionization density of the crystal.[2]

About 15% of photoelectrons are produced by the fast component, whereas 85% are produced from the slow component.[2] The total number of photons emitted by a BaF_2 crystal is about 12 per keV of photon energy.[2] The ratio between the intensity of the fast and slow scintillation components of BaF_2 depends on the interaction characteristics of the incident particle.[2] Pulse shape discrimination techniques are used to provide gamma discrimination and particle identification. BaF_2 detectors can be used for pulse shape discrimination to discriminate the charged particles from neutron particles (gamma rays and neutrons).[3] The scintillation intensity of the fast component is independent of temperature between -40 ℃ and 25 ℃. The slow component is known to vary slowly as temperature changes, with a maximum at -10 ℃.[2]

Based on previous work by the authors W Egger, P. Sperr and G Dollinger, the time and energy resolution were evaluated of four different scintillator materials, BaF_2, BC-418, LYSO, and $CeBr_2$ at a gamma energy of 511 keV.[18] Each scintillator was a cylinder with a diameter of 25 mm and a height of 10 mm, and the data were collected by using the Photonics XP2020/URQ photomultiplier tube.[18] For the time resolution measurements experimental setup and method, the researcher employed a conventional fast-slow arrangement (see Figure 11). A Na-22 source was placed between the timing and reference detectors.[18]

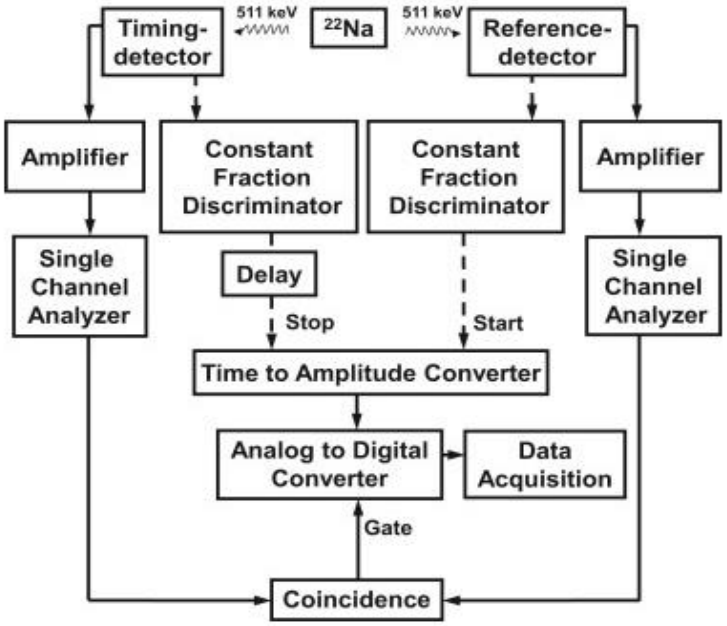

Figure 11. Fast-slow configuration**.** Reprinted from [W.E.U.A.P.S.G.D. (2015b). Time- and energy-resolution measurements of BaF2, BC-418, LYSO and CeBr3 scintillators. *Nuclear Instruments and Methods in Physics Research Section A: Accelerators, Spectrometers, Detectors and Associated Equipment*, *786*(0168–9002), 5–11.]

The fast circuit (dashed lines) converts the detector time signals to start and stop signals for the ORTEC 566 Time to Amplitude Converter using a double Constant Fraction Discriminator (CFD).[18] In the slow circuit, an energy window is established.[18] The detectors' energy signals are amplified with an ORTEC 855 Dual Amplifier (DA) and 511 keV events are selected using ORTEC 551 Timing Single-Channel Analyzers (SCAs). The SCA signals are routed through a Canberra 2144A Fast/Slow Coincidence.[18] The coincidence module's output is used to generate the gate signal for the Canberra 8701 Analog to Digital Converter (ADC). As a result, the time difference between the start and stop signals from the CFD is measured. These values contribute to forming a time distribution that can be characterized by a Gaussian function, as illustrated in Figure 12.[18]

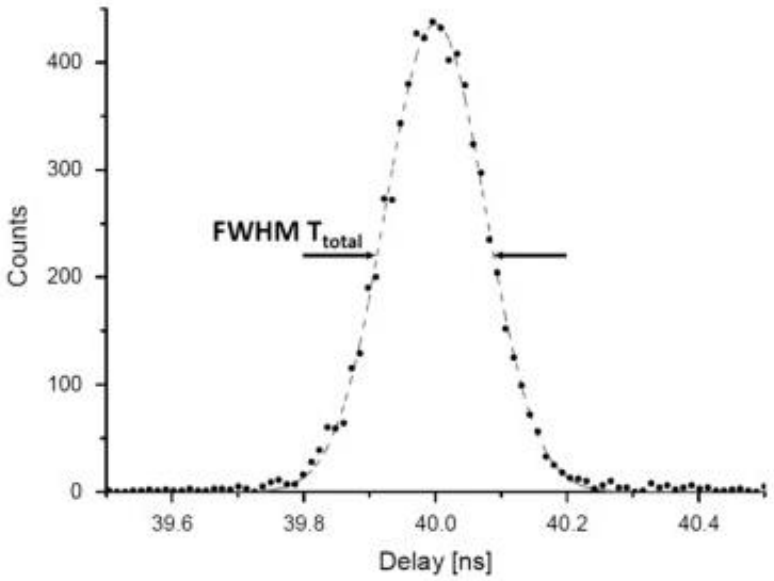

Figure 12. Typical shape of time distribution Reprinted from [W.E.U.A.P.S.G.D. (2015b). Time- and energy-resolution measurements of BaF2, BC-418, LYSO and CeBr3 scintillators. *Nuclear Instruments and Methods in Physics Research Section A: Accelerators, Spectrometers, Detectors and Associated Equipment*, *786*(0168–9002), 5–11.]

The quantity that can be deduced from the time distribution is the full-width-at-half-maximum (FWHM) T_{Total}, which will be referred to as total time resolution.[18] Thus, by knowing the reference-single detector's time resolution T_{Ref} (FWHM), one may deduce the appropriate timing-detector configuration's single time resolution T_{Timing} (FWHM) from the relation.[18]

A three-step optimization technique is used to identify the best single time resolution for each photomultiplier–scintillator configuration.[18] The result of the time resolution measurements is shown in Figure 13 to Figure 15 and indicates the dependence of T_{Timing} on CFD delay, CFD threshold, and timing-detector supply voltage.[18] In the first step, the optimization CFD delay is determined for each of the four timing-detectors using a steady CFD threshold of 50 mV and a constant timing-detector supply voltage of +2200 V (see Figure 13).[18] The optimal T_{Timing} values

for BaF_2 and BC-418 are 1.9 ns and 2.5 ns, respectively.[18] The high T_{Timing} value for BaF_2 at t_d = 4.25 ns is due to a 4.25 ns delay which is too long for the BaF_2-detector time signal's narrow signal width of only 4 ns. T_{Timing} has the best time resolution for LYSO and $CeBr_3$ at 1.0 ns.[18]

In the second step, the time resolution is optimized by varying the CFD threshold at the optimal CFD delay values for each timing-detector combination shown in figure 14.[18] The supply voltage to the timing detector is kept constant at +2200 V.[18] The optimal CFD threshold values for BaF_2, BC-418, LYSO, and $CeBr_3$ are 150 mV, 400 mV, 30 mV, and 30 mV, respectively (Figure. 5). As illustrated in Figure 14, the T_{Timing} values fluctuate only slightly.[18] This indicates that the single time resolution should be relatively insensitive to the CFD threshold as long as the energy window (defined in the SCA) is greater than the CFD threshold.[18] The third step, the timing-detector supply voltage (Figure 15) is optimized with the best values of the CDF delay and CFD threshold values for each timing-detector design, respectively.[18] The greatest T_{Timing} values for BaF_2 and BC-418 are discovered at +2200 V, whereas the best values for $CeBr_3$ and LYSO are discovered at +2600 V.[18]

To sum up everything that has been stated, BaF_2, BC-418, LYSO, and $CeBr_3$ have optimum single time resolutions (FWHM) of 119 ps, 117 ps, 269 ps, and 127 ps, respectively.

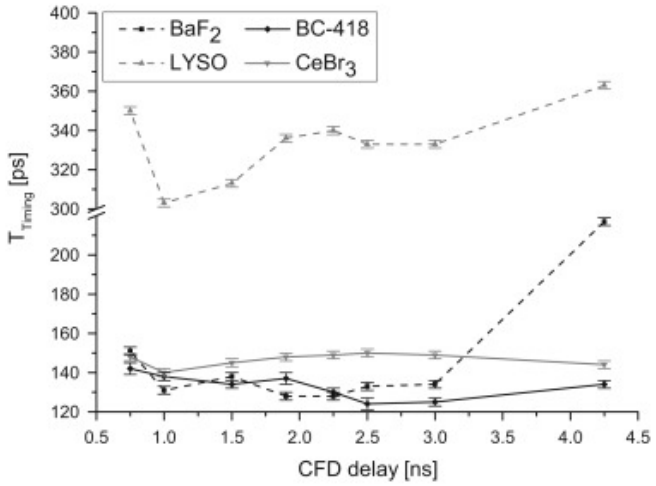

Figure 13. Single time resolution T_{Timing} as function of the applied CFD delay. The CFD threshold was set to 50 mV and the Timing-detector supply voltage was +2200 V. Reprinted from [W.E.U.A.P.S.G.D. (2015b). Time- and energy-resolution measurements of BaF2, BC-418, LYSO and CeBr3 scintillators. *Nuclear Instruments and Methods in Physics Research Section A: Accelerators, Spectrometers, Detectors and Associated Equipment, 786*(0168–9002), 5–11.]

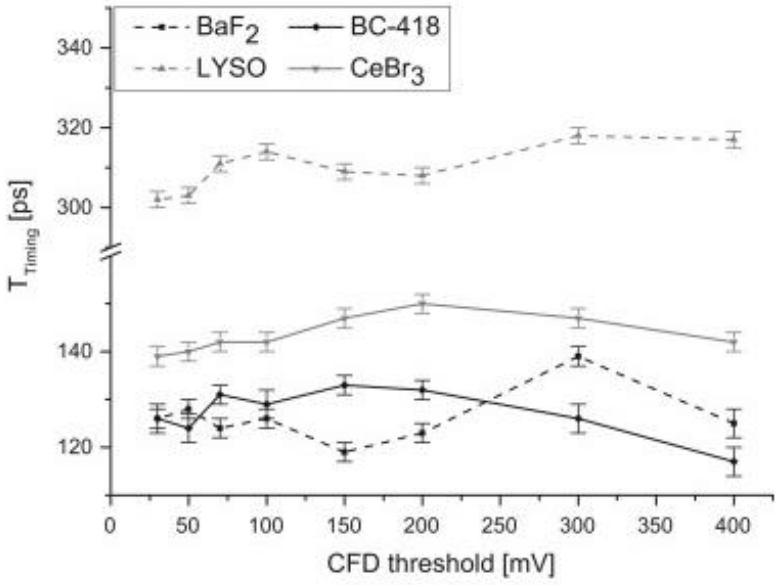

Figure 14. Single time resolution T_{Timing} as function of the used CFD threshold at the optimal CFD delay. The Timing-detector supply voltage was +2200 V. Reprinted from [W.E.U.A.P.S.G.D. (2015b). Time- and energy-resolution measurements of BaF2, BC-418, LYSO and CeBr3 scintillators. *Nuclear Instruments and Methods in Physics Research Section A: Accelerators, Spectrometers, Detectors and Associated Equipment, 786*(0168–9002), 5–11.]

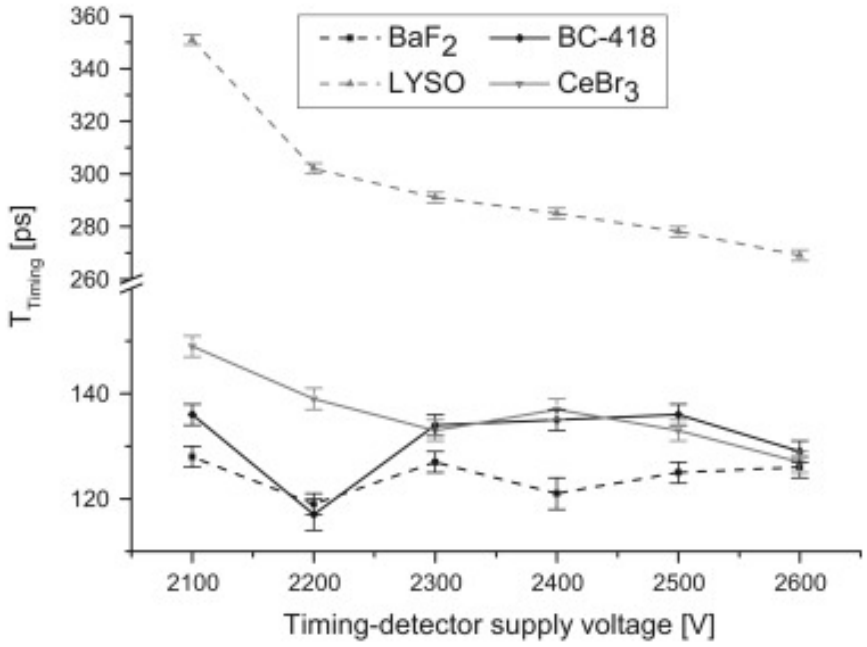

Figure 15. Single time resolution T_{Timing} as function of the Timing-detector supply voltage at the optimal CFD delay and optimal CFD threshold. Reprinted from [W.E.U.A.P.S.G.D. (2015b). Time- and energy-resolution measurements of BaF2, BC-418, LYSO and CeBr3 scintillators. *Nuclear Instruments and Methods in Physics Research Section A: Accelerators, Spectrometers, Detectors and Associated Equipment*, *786*(0168–9002), 5–11.]

For energy resolution ΔE/E measurements (ΔE is the FWHM of the 511 keV photopeak), the timing-detector energy signal is supplied into the DA, which is then immediately processed by the ADC.[18] The energy resolution is reported in this work only for the timing-detector supply voltage where the time resolution T_{Timing} was optimal.[18] The ^{22}Na energy spectrum is measured for each timing-detector configuration at the timing-detector supply voltage that provides the optimum single time resolution. The energy resolution of photomultiplier–scintillator setups that exhibit a photopeak in the energy spectrum is determined. BaF_2, LYSO, and $CeBr_3$ have energy resolutions of 9.8%, 9.7%, and 5.4%, respectively. BC-418's energy spectrum reveals no photopeak at 511 keV due to its low density of around 1 g/cm3 and low effective atomic number.

$CeBr_3$ appears to be the most promising material for simultaneously measuring time, energy, and position resolution in positron annihilation studies, due to its excellent time and energy resolution features.[18]

The process is used by CoMPASS to determine what voltage spike is a pulse is called CFD. This technique finds the timetag of a pulse at a point when the amplitude reaches a fixed fraction of the full amplitude. This works by taking each input waveform and attenuating them by a factor *f*, equal to the desired timing fraction of their full amplitude. Then these signals are inverted and delayed by a time *d*, equal to the time it takes the pulse to rise from the constant fraction level to the pulse peak. These two types of signals are added together to generate a bipolar pulse, the CFD, and its zero-crossing (corresponding to the fraction f of the input pulse) is used as the timetag. Possible choices of attenuation are: 25%, 50%, 75%, and 100% (i.e., no attenuation) with respect to the input amplitude. The sample-before-zero-crossing (SBZC) and the sample-after-zero-crossing (SAZC) are the samples before and after the zero crossing (in case of interpolation they are the n-th samples before and after the ZC). The SBZC is equivalent to the Coarse Time Stamp (T_{Coarse}), which is the trigger timestamp as determined by the standard PSD algorithm (leading edge). The value of the fine-time-stamp (T_{fine}) is calculated as the linear interpolation of the SBZC and the SAZC according to the formula:

$$ZC = T_{coarse} + T_{fine} \qquad \text{Eq. (4)}$$

$$T_{fine} = \frac{midScale - SBZC}{SAZC - SBZC} * T_{SAMPLE} \qquad \text{Eq. (5)}$$

Where the midScale corresponds to whichever value is acting as the baseline of the pulse and T_{Sample} is the sampling period of the digitizer series which in this case is 4 ns (DT5730). The

"Interpolated Zero Crossing" (ZC) then corresponds to the sum of the coarse timestamp and the fine timestamp as shown in Eq. (4).

Based on previous work by the authors H. Nabielek, M. Liu, the fast and efficient burnup measuring system (BUMS) for irradiated spherical fuel elements is needed for pebble bed HTGR (high temperature gas cooled reactors) with a multi-pass system.[19] As illustrated in Figure 16, during the reactor operation, spherical fuel elements inserted at the top of a pebble bed flow downward. They are evaluated for mechanical integrity and burnup after being removed from the bottom.[19] Next, they are reloaded from the top of the core if the pebbles are in good condition and the targeted burnup has not been reached. Typically, the system is limited to over 55 hours of cooling time and 10 seconds of measurement time for each pass through the system. These constraints make collecting and analyzing high accuracy gamma spectra difficult in general.[19]

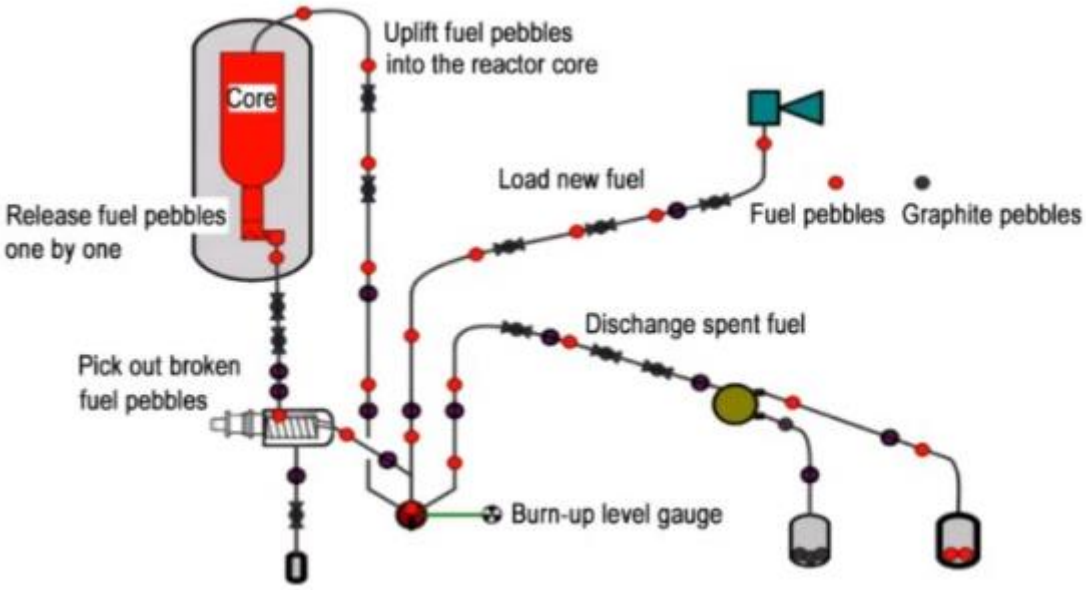

Figure 16. Recirculation of spherical fuel elements in a modern HTGR. Reprint from [H.N.M.L.B.L. (2020). Burnup measurement error analysis of HTR fuel spheres using ab-initio Monte-Carlo simulations, *Nuclear Engineering and Design, 363*(0029–5493).]

The purpose of this research paper is to use simulation analysis to investigate the constraints of using BaF_2 for fast burnup measurements.[19] The gamma spectrum collection is simulated using a Monte-Carlo simulation method.[19] When typical gamma measurement devices are used, researchers determine that the one-sigma relative statistical uncertainty is 6.5 % at the ultimate 200 MWth MODUL burnup of 9.2 % FIMA. This FIMA uncertainty range is a result of the limiting statistics of a very short measurement time and the concurrent interference of neighboring peaks during such short cooling times.[19] In this paper, the ^{140}La caused Compton edge, which influenced the background near the ^{137}Cs peak, was taken into account for the first time. The relative statistical error could be brought down to 2–3%, with longer cooling time and longer measurement time.[19] The longer cooling time could reduce peak interference and the longer measurement time will improve statistics.[19] However, one remaining problem is the study of the system's count rate limit in order to avoid peak shifts, peak broadening, and the harmful impacts of pulse pile-up and dead time. It was suggested that one may enhance the count rate by using better Ge detectors and simultaneously measuring with more detectors, which should be considered in real-world HTGR engineering measurements.[19] In this experiment, the ^{137}Cs 30 has a 30.2-year half-life and a relatively high fission yield, 6.7%, therefore the ^{137}Cs peak at 661.6 keV provides a credible measure of accumulated burn-up. Since the 1960s, when Ge semiconductor detectors introduced high-resolution spectrometry, gamma-spectrometric observations of the ^{137}Cs peak have been utilized in HTGR technology.[19] Also, the random production of Gaussian gamma peaks is used to replicate the observations and to determine statistical uncertainty through multiple applications.[19]

The Burnup Determination

Burnup is defined as the energy generated per unit mass of fuel and is typically referenced in units of megawatt days per metric tons of uranium (MWD/MTU). Consequently, it is directly proportional to the rate of fission in a given fuel element.[5] Ideally, burnup could be computed directly by measuring the distribution of fissile material remaining in the fuel. However, this method of passive nondestructive measurement is not capable of yielding that information directly. This is due to the extremely high radiation sources in irradiated fuel that will subdue the fissile material's direct signatures. Therefore, passive burnup measurements are performed indirectly by observing the spontaneous emission of gamma and neutron radiation from the fission products and heavy actinides produced when the fuel is irradiated.[5]

Based on previous work by the authors J. Chen, A. Hawari, gamma-ray spectrometry analysis of pebble bed reactor fuel using Monte Carlo Simulation. The modular pebble bed reactor (MPBR) contains approximately 360,000 fuel pebbles that are continuously circulating through the core.[5] Each pebble may contain a total of 7–9 g of UO_2 enriched to approximately 8% in ^{235}U.[5] The fuel was assumed to go through 120 days of irradiation and 40-hr cooling for each period.[5] Also, ORIGEN 2.1 code simulated the circulation of the pebbles in and out of the core in MPBR. In the simulation a 100% efficient high-purity coaxial germaium (HPGe) detector was assumed, with a pebble placed at 100 cm from the detector and accounted for Gaussian broadening of the gamma-ray peaks.[5] Once the burnup reaches 80,000 MWD/MTU, the pebble is discharged.[5] Moreover, to simulate different levels of burnup, a unique source term was also created at the burnup steps of 20,000, 50,000, and 80,000 MWD/MTU.[5] Based on the previous studies when the fuel went through 120 days of irradiation and 40-hr cooling, the isotopes of ^{137}Cs, ^{60}Co

and ^{134}Cs could be utilized as relevant resistant burnup indicators. Monte Carlo method was used to simulate a pebble gamma-ray spectrum at 80,000 MWD/MTU. There are several hundred radionuclides were produced. However, many of these radionuclides were excluded from consideration because of their low activities and/or extremely weak gamma rays.[5] In addition, several radionuclides were excluded because they were not gamma-ray emitters. Consequently, by combining the activities and intensities of the major gamma-rays from these radionuclides, a source probability distribution function was created for utilization in the Monte Carlo calculation.[5]

It was concluded that the 1173 keV peak of ^{60}Co is overwhelmed by the 1173 keV peak of ^{132}I.[5] However, the 1333 keV peak seems free from interference, which allows it to be used for burnup determination. In this scenario, the 1333 keV peak can be combined with the 605 keV peak of ^{134}Cs to form a burnup indicator that is based on the correlation of the relative activity of ^{60}Co to ^{134}Cs with burnup.[5] Additionally, Monte Carlo simulations were performed to produce the gamma-ray spectra at 20,000 and 50,000 MWD/MTU. In both cases, the peak intensities were lower, but the observed trends were similar to those observed at 80,000 MWD/MTU.[5]

Based on previous work by the authors I. Hossain, N.Sharlp and K.K. Viswanathan, gamma rays are generally characterized as high energy radiation and short wavelengths within the electromagnetic spectrum.[10] It is normally blocked by material of higher atomic number and density as they can be damaging when absorbed by living cells.[10] The energy dependence of efficiency and resolution of HPGe and sodium iodide (NaI) detectors using gamma-ray spectroscopy is necessary.[10] To quantify the efficiency variation as a function of energy, measurements have been made on several coaxial detectors of various crystal types and sizes in

different geometries.[10] The average value of the FWHM corresponds to the resolution of the high purity germanium (HPGe) and (NaI) detector.[10] It describes how useful the detector is for clearly separating two adjacent energy peaks and hence, for differentiating between different nuclides. Both detectors, HPGe and NaI, showed a similar behavior with FWHM increasing with gamma-ray energy.[10] However, the FWHM for the HPGe detector has been observed to be smaller, so it can be said to offer very good resolution and is a useful instrument for nuclide identification when compared to the NaI detector.[10]

The detector's diameter and thickness define the sensitivity.[10] Thickness directly influences the energy beyond which the efficiency starts to decrease sharply. As gamma-ray energy increases, the efficiency has been observed to decrease exponentially. Despite the similar trends, the efficiency of NaI has been observed to be much higher than that of HPGe due to its large area detector and therefore has a high probability of detecting gamma radiation.[10] The HPGe detector offers less detection efficiency compared to the NaI detector.[10] This means that HPGe is efficient in detecting nuclides with lower energy but not nuclides at higher energy.[10] The NaI detector is a more efficient detector compared to the HPGe detector although it has a very poor resolution. HPGe detectors have better resolution compared to the scintillation type of detector, NaI. The HPGe detector offers the advantage of resolving two closely located energy points and has the ability to detect a mixture of fissile material. Even though HPGe has a very good resolution, it is less efficient than the NaI detector. Its efficiency decreases exponentially with energy and only detects nuclides with lower energy rather than nuclides at higher energy.[10]

Comparison of Characteristics of NaI and BaF_2 Detector

Table 3 compares the characteristics of inorganic scintillation detectors NaI and BaF_2. BaF_2 has a higher density than NaI, meaning there are more atoms inside the material, increasing the probability of gamma interaction. Also, compared to the size of the detector in table 3, the BaF_2 detector is almost double the size of NaI. Based on the definition of intrinsic efficiency, being the ratio of the number of photons detected to the number of photons incident on the detector surface, the bigger size of the detector could capture more photons and then have a higher detector efficiency. However, the parameter of the photoelectron yield (% of NaI) says if the NaI detector was a standard detector with 100% photoelectron yield, then BaF_2 would only have a total of 19 % including fast and slow components.[31] Figure 17 shows the wavelength intensities of absorption, fluorescence, and phosphorescence spectrums. The excitation spectrum is seen in red, being identical to the absorption spectrum because if the fluorescence emission has to occur, radiation must be absorbed to create an excited state. The spectrum in blue represents fluorescence and green spectrum represents phosphorescence. The BaF_2 emitted fast (fluorescence) and slow components (phosphorescence) are known; the fast component having a max wavelength emission at 220 nm, and the slow component having a max wavelength emission at 310 nm.[30] Therefore, it can be determined that most photons emission were located in the absorption spectrum, and only a few photoelectrons occur in the detector. Conversely, because the NaI has a longer wavelength which is 450 nm, the photon emission will be very high.[32]

Table 3. Compares the characteristics of inorganic scintillation detectors NaI and BaF_2.[30 31]

	NaI	BaF_2
Material	Inorganic scintillation detector	Inorganic scintillation detector
Density (g/cm^3)	3.67	4.88
Wavelength of emission max (nm)	450	220 (fast) 310 (slow)
Time response (ns)	230	0.8 (fast) 630 (slow)
Energy resolution at 661.7 keV (%)	6	15
Abs.Light yield(photons/keV)	38	1.9 (fast) 10 (slow)
Photoelectron Yield (% of NaI)	100	3 (fast) 16 (slow)

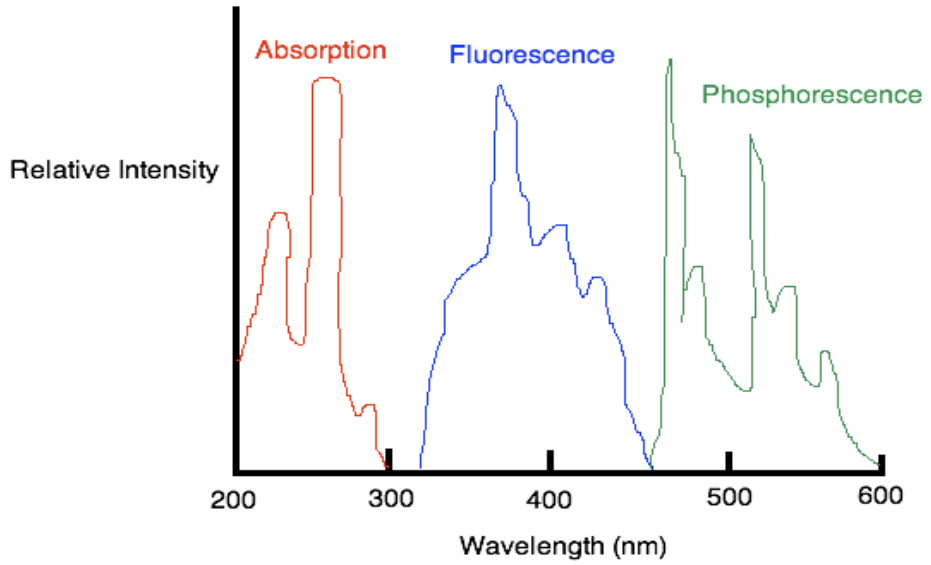

Figure 17. Wavelength intensities of absorption, fluorescence, and phosphorescence of an arbitrary scintillator. Reprint from [Libretexts. (2020, August 15). *Fluorescence and Phosphorescence*. Chemistry LibreTexts.]

V. METHODOLOGY

To explore the energy resolution characterization for gamma-spectroscopy. The high voltage (HV) determination and energy calibration had to be accomplished before the real measurement. For the HV determination, an investigation was done for high voltages 2.0 kV, 2.1 kV, 2.2 kV, 2.3 kV, and 2.4 kV. Then, the gamma-ray energy spectrum of BaF_2 showed the photopeak of ^{137}Cs and ^{60}Co with different high voltages. After the energy calibration, using the high voltages listed above, the optimum energy resolution was determined with an FWHM calculation.

The analog to digital conversion (ADC) has 16,384 energy channels corresponding to the counts for the digitizer used in this research. All these energy bins were broadened to the Gaussian pulses and eventually summed up. A MATLAB script was created to carry out the mathematical operation of convolution. The spectrum used is from Xenon-100, provided by X-Energy.

Objective 1: Explore the energy resolution characterization for gamma-spectroscopy.

a. The optimal HV is determined for the BaF_2 detector.
b. ^{137}Cs and ^{60}Co are used to calibrate the BaF_2 detector.
c. Find the optimum energy resolution for the BaF_2 detector.
d. Implement the resolution spectrum onto the pebble bed spectrum by broadening the energy peaks.

To explore the time resolution of the barium fluorine for fast measurement, a one microcurie ^{137}Cs was used to do the 30-minute measurement at 2.1 kV, and data was collected by CAEN's DT5730 digitizer using the CoMPASS software. Then, a python code was written to

process the collected data, fit various pulses to the exponential curve, and determine the fast and slow components of BaF_2. Eventually, the fast component curve was chopped out to investigate the rising time and time characteristics of BaF_2.

Objective 2: Determine the time resolution of the fast response for a Barium Fluoride (BaF_2) detector.

a. Measure data collected with CAEN's CoMPASS software connected to the BaF_2 detector.
b. Process the CoMPASS raw pulse data into useful format for the further analysis.
c. Fit the exponentials curve to figure out the fast and slow components of the detected pulses.

V.A. Explore Energy Resolution Characterization for Gamma-Spectroscopy.

V.A.1-3 The optimal HV is determined for the BaF_2 detecotr, ^{137}Cs and ^{60}Co are used to calibrate the detector and eventually find the optimum energy resolution.

This procedure involved the use of radiation detection and counting statistics analysis. Such a process uses detectors, digitizers, and data acquisition software. This equipment came from Dr. Prasad's Neutron Sensing Laboratory and Dr. Yennello's Group in the Cyclotron Institute at Texas A&M University. The equipment borrowed from the Cyclotron Institute consisted of one BaF_2 detector (AM10), a 10 DB attenuator, a 50 Ohm terminator, and a BNC terminator. The procedure listed was carried out for each of the voltages stated earlier with the only variation being that voltage value change.

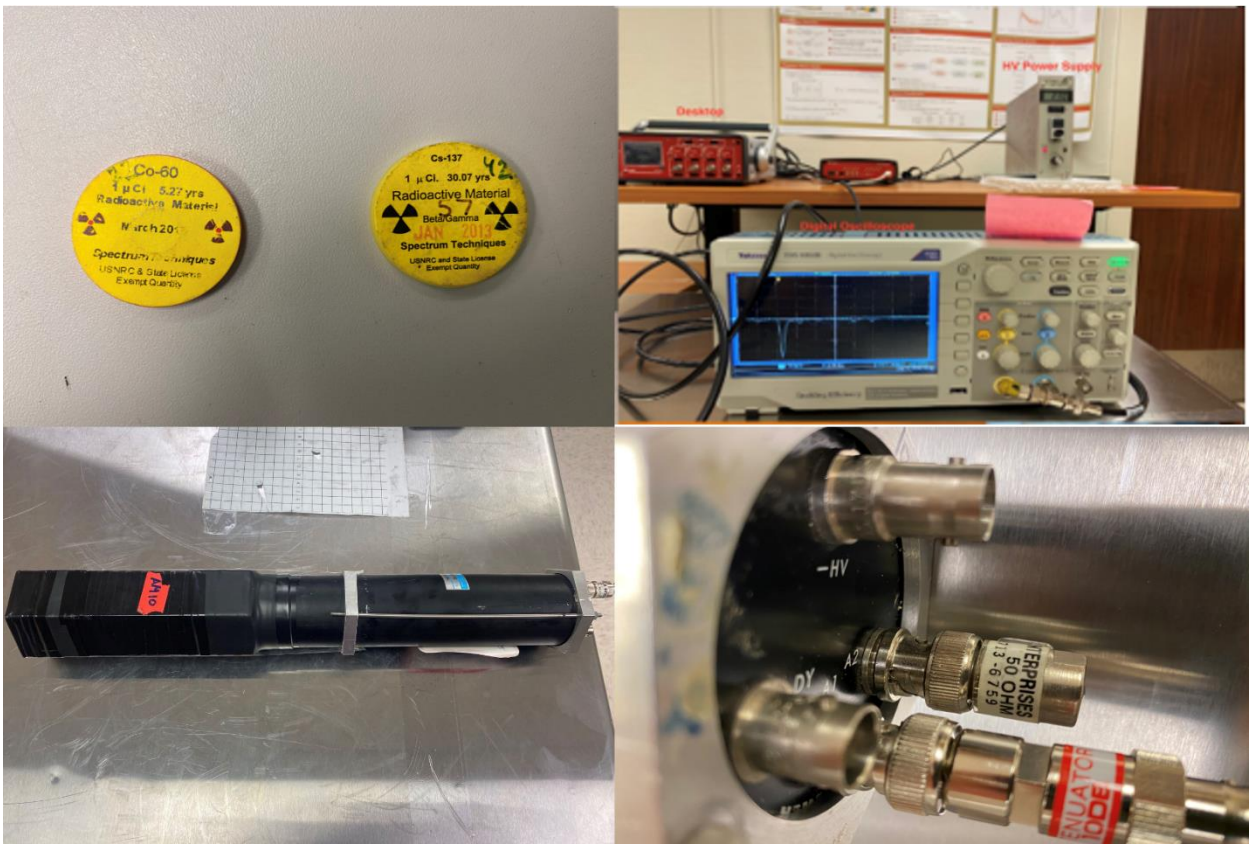

Figure 18. Materials used in measurements including ^{137}Cs and ^{60}Co test source (top left), TBS1052B Digital Oscilloscope (top right), BaF_2 detector (bottom left), and BaF_2 detector cable connections (bottom right).

As shown in Figure 18, a Mirion HV Power Supply Model 3002D was used as it allowed for a negative voltage. It was connected to the BaF_2 detector through the -HV connection and the knob turned from positive to a negative voltage. The BaF_2 was connected to a TBS1052B Digital Oscilloscope to visualize the pulses and check that the frequency values matched expectations. This connection involved the 10 DB attenuator connecting directly to the BaF_2 detector through connection A1. Then a cable connected the 10 DB attenuator to the BNC terminator, which was connected directly to the digital oscilloscope through the 300V CAT II channels. The pulses

were visualized by changing the vertical, horizontal, and threshold voltage knobs on the oscilloscope. Steadily moving a ^{137}Cs source directly away from the detector, the frequency values were observed to decrease greatly (example. 1.87 kHz to 650 Hz).

CAEN's CoMPASS Software was then used for spectroscopy analysis. Connection A1 was disconnected from the BaF_2 detector and using a singular cord CAEN's Desktop Digitizer DT5730 was connected to the BaF_2. Digitizer DT5730 was connected to a lab computer that had CAEN's CoMPASS Software downloaded. ^{137}Cs and ^{60}Co sources were used for energy calibration. First, a ^{137}Cs source was placed 2 cm away from the BaF_2 detector with lead shielding surrounding both the source and the entire hexagonal region of the detector. Using CoMPASS, a 5-minute run was conducted, and the detector energy was calibrated. Then a ^{60}Co source was added to the system and another 5-minute run was conducted to confirm energy calibration. Finally, the ^{60}Co source was removed from the system and a 20-minute run (accompanied by a 20-minute background run) was conducted with just the ^{137}Cs. From this run, the photopeak and channel number were recorded. The background was subtracted from the data, the full width half maximum (FWHM) was calculated, and then the energy resolution percentage was calculated (energy resolution percentage (%)) = (FWHM / Channel No. ×100%).

V.A.4. Implement the Resolution Spectrum onto The Pebble Bed Spectrum by Broadening the Energy Peaks.

Broadening the pulses allows for the energy resolution of each energy per channel to be correctly represented. The energy resolution influences the width of each channel energy, which in turn influences the subsequent results. By accounting for this energy resolution, a clearer

energy per channel can be displayed. The result of the broadened spectrum can be seen in the result and analysis section.

Convolution is used with the Gaussian function to broaden each of the gamma-ray photopeak to those seen from the BaF_2 detector. The resolution is measured in the lab, and a broadened spectrum from the pebble is computed. Convolution is a mathematical operation on two functions that produces a third function which expresses how the shape of one is modified by the other. It can be defined as the integral of the product of the two functions after one is reversed and shifted. The integral is evaluated for all values of shift, producing the convolution function. This convolution function corresponds to the probability density function set up by Gaussian function and shown in Eq. (9).

In probability theory, a probability density function (PDF) of a Gaussian was used to simulate the PDF for a photopeak's energy distribution. These distributions are symmetric about their mean, and are non-zero over the entire real line, appearing as a bell curve. The value of the normal distribution is practically zero when the value x lies more than a few standard deviations away from the mean. Due to this reason, the use of convolution does not always increase the surrounding values by large margins, as a sample's probability density function can have a low percentage chance of affecting a surrounding sample.

For the digitizer used (DT5730), the analog to digital conversion (ADC) has 16,384 energy channels corresponding to the counts. All these energy bins were broadened to the Gaussian pulses and eventually summed up. The probability density function is shown in Eq (9).

The sigma was calculated by Eq (8), where the energy resolution (ER) for the BaF_2 is around 15% and E is presented in each energy bin. Eq. (8) was deduced from Eq. (6) and Eq. (7). The variable μ represents the energy bin which is being broadened. When E_1 is being broadened, μ equals E_1. However, when the energy bins are being broadened, the contribution falls in other bins too. This means x will vary from E_1 to E_n.

$$\text{Energy Resolution} = \frac{\text{FWHM}}{\text{E}} \qquad \text{Eq. (6)}$$

$$\text{FWHM} = 2.355\sigma \qquad \text{Eq. (7)}$$

$$\sigma = \frac{ER * E}{2.355} \qquad \text{Eq. (8)}$$

$$\text{f(x)} = \frac{1}{\sigma \cdot \sqrt{2\pi}} \cdot \text{e}^{-\frac{1}{2}\left(\frac{\text{x}-\mu}{\sigma}\right)^2} \qquad \text{Eq. (9)}$$

$$\begin{pmatrix} Sum-up \\ Counts \\ \vdots \end{pmatrix} = \text{E}_1\ (\text{Counts}) * \begin{pmatrix} f(x) \\ E1 \\ \vdots \end{pmatrix} * \Delta E * 0.001 + \text{E}_2\ (\text{Counts}) * \begin{pmatrix} f(x) \\ E1 \\ \vdots \end{pmatrix} * \Delta E * 0.001 + \ldots + \text{E}_{n^*}$$

$$*(\text{Counts}) * \begin{pmatrix} f(x) \\ E1 \\ \vdots \end{pmatrix} * \Delta E * 0.001\#$$

Eq. (10)

After that, a MATLAB script was created to carry out the mathematical operation of convolution as characterized by Eq. (9) and Eq. (10). The script reads energy and counts data for each channel and groups them into matrices. A double "for loop" is used to read through each channel and energy values used Eq. (9). Inside the for-loop Eq. (6), Eq. (7), and referenced energy values from the earlier mentioned matrix are used to calculate Eq. (8). Then Eq. (9) is used along with the energy values to calculate the probability density function. It is important to

understand that the second for loop inside the first is necessary to perform (x-μ) where x is every single channel's energy value, and the resulting Eq. (9) solution becomes a matrix as seen in Eq. (10). Now, using the results of Eq. (9) and the other inputs of Eq. (10), the summation is conducted. The change in energy ΔE equals ($E_n - E_{n-1}$) for every summation of energy channel n except for the first channel at which the E_{n-1} is assumed to be 0 MeV.

V.B. Determine the Time Resolution of the Fast Response for A Barium Fluoride (BaF2) Detector.

Table 4. The original raw pulse data with 25% constant fraction discriminator (CFD) output by CoMPASS

Timetage	Calib Energy	Energy Short	Flags	Samples	Total 496 Samples for Each Timetage	
1141808564	195	33	0*4000	8068	⋯	8130
1142918736	71	23	0*4000	8072	⋯	8134
⋮	⋮	⋮	⋮	⋮	⋮	

Table 5. The processed raw pulse data with 25% CFD output by using a python algorithm.

Time1(ns)	Pulse1(mV)	Time2(ns)	Pulse2(mV)	⋯	Time8192(ns)	Pulse8192(mV)
114714.5	1.71	1142824.7	1.58	⋯	1058436755	1.95
114716.5	1.71	1142826.7	1.58	⋯	1058436757	1.95
⋮	⋮	⋮	⋮	⋮	⋮	⋮

The raw data that CoMPASS outputs were processed into a usable and relevant format using python code developed in Dr. Prasad's Neutron Sensing Laboratory by Xiaodong Tang and Benjamin Wellons. The data was outputted from CoMPASS in CSV files of the format seen in Table 4. This format has each successive row represent a pulse detected by the detector, which is then filtered through CoMPASS's parameters to be listed as an official pulse. Each pulse is given

a timetag which signifies the point of zero crossings at which the pulse was officially recorded. The timetag are given in picoseconds (ps) and are accurate by plus or minus two ps as per the digitizer used (DT5730). The columns labeled Calib_Energy, Energy Short, and Flags are not relevant to the analysis conducted and can be therefore overlooked. The columns starting with the label SAMPLES are then the values that make up the pulse. These values are given in ADC units, known in CoMPASS as the least significant bits (LSB). An example of a pulse as given by CoMPASS can be seen in Figure 19. Each pulse consists of 496 sample values at a resolution of 2 ns. The DT5730, however, was set to only have a sampling rate of 4 ns, so there are only 248 unique data points. The outputted files were shown in Table 5, and SAMPLE columns simply repeat every two. These files are then processed with Python code outputting CSV files, as seen in Table 5. This processing was conducted with a python script named "Compass_Pulse_Data_Developement." The script's overall purpose is simply to flip the pulses, convert their units to mV, and create relevant time data corresponding to each sample point. It starts by determining the total number of pulses detected by CoMPASS over the acquisition window along with confirming the length of each pulse's sample data. This allows for the preallocation of numpy arrays of zeros which can later be filled with pulse and time data. Preallocation is useful as it saves computing time for large data sets. Now CoMPASS' CSV files are opened and read through line by line allowing for the manipulation of data in each line to be completely carried out and then stored in the previously mentioned numpy arrays. To correct the pulses from ADC units to mV, the baseline value of the pulse must be found such that the pulse can be pulled down to 0 on the y-axis. For this code, the baseline was found to be the maximum value of each pulse listed. As seen in Figure 20, the maximum value of each pulse will

technically correspond to the minimum value once the pulse is flipped. This way the pulse can be corrected to a zero-axis value without the loss of any sample data points.

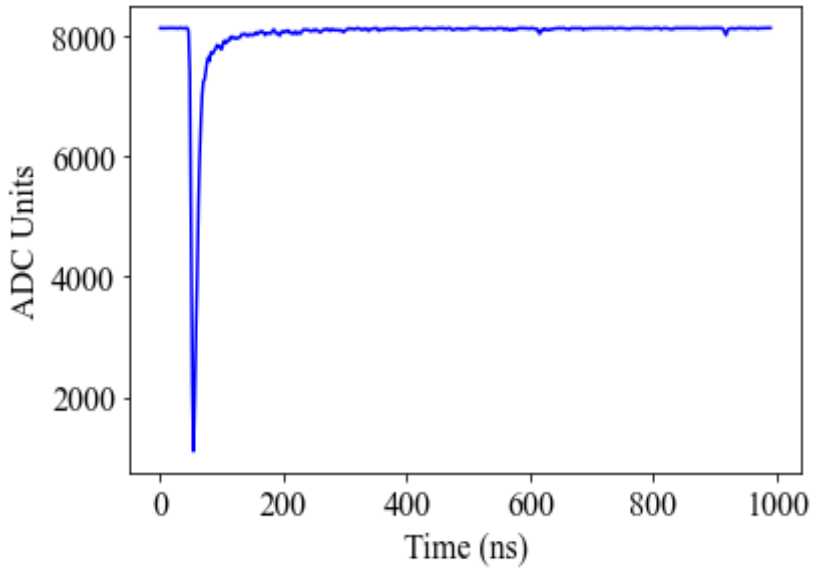

Figure 19. An example of an original pulse as given by CoMPASS

With the baseline found, the values in each pulse are multiplied by -1 to flip them, added to the baseline such that their values will be positive, and finally multiplied by 0.1220703125 to convert them from ADC to mV. This conversion factor comes from the number of channels total along with the selected input dynamic voltage. The input dynamic voltage is set at 2 Volts which becomes 2000 mV. Then this value is divided by the total number of channels on the digitizer, being 16,384, to get the conversion value listed. Once the pulses are properly upright, they appear as in Figure 4. These corrected pulses are placed into the arrays to be used further. Numpy arrays are handy for storing data because they can be mathematically manipulated and referenced easily in python.

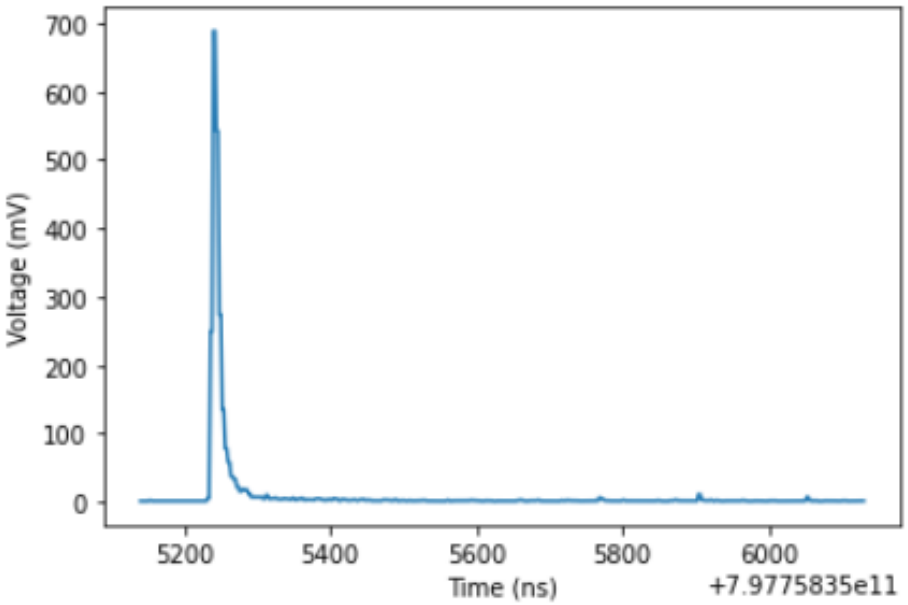

Figure 20. An example of corrected pulse when the maximum value of each pulse will technically correspond to the minimum value once the pulse is flipped.

Each corrected pulse's maximum height is now found to be used in determining at which point the pulse corresponds to the given timetag. The process used by CoMPASS to determine what voltage spike is actually a pulse is called constant fraction discrimination (CFD). This technique sets the timetag of a pulse to the time when the amplitude reaches a fixed fraction of the full amplitude. It works by taking the input waveforms and attenuating them by a factor f, equal to the desired timing fraction of full amplitude. Then the signals are inverted and delayed by a time d, equal to the time it takes the pulse to rise from the constant fraction level to the pulse peak. These two forms of signals are summed to produce a bipolar pulse, the CFD, and its zero-crossing – corresponding to the fraction f of the input pulse – is taken as the timetag. This process can be observed in Figure 21. In the recorded run, the fraction f was set to 0.25 and the delay d to 6 ns. The 25% value was selected after a trial run with multiple available percentages

(25%, 50%, 75%, and 100%). The time delay of 6 ns was selected as it is the average time taken for a pulse to go from beginning its rise to its maximum height.

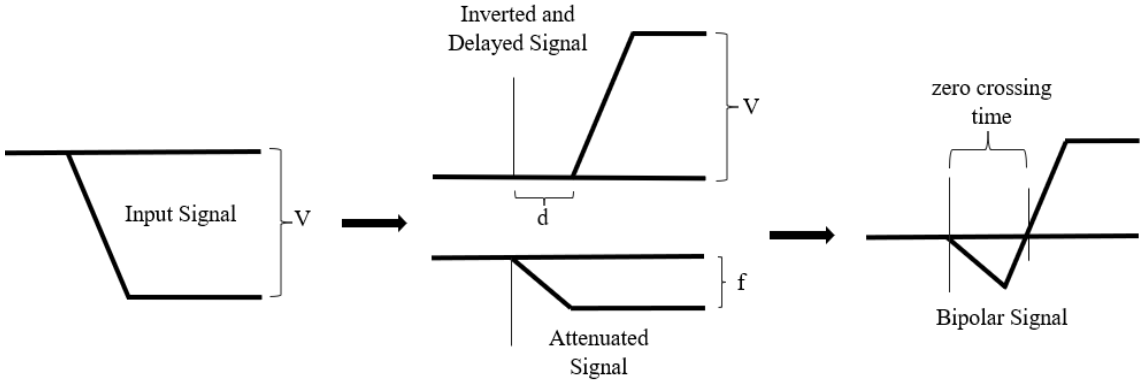

Figure 21. The process of to determine the beginning of the timetag value since the value of CFD was known as 0.25.

Understanding the use of the delay and fraction, the timetag corresponding values were found by setting it equal to which pulse's sample passed 25% of the pulse's maximum height. This method allowed for a more computationally quick way of assigning the timetag to a sample. Once the index of the timetag was recorded, a numpy array of counting numbers was created. This array would start at the negative value of the timetag index and extend to 496 values. Then it would be multiplied by two such that the interval of two ns recording rate would be preserved. Finally, the timetag, converted from ps to ns, would be added to the array and created an array that changed to and from the timetag by intervals of 4 ns. Now that the corrected pulse data and their corresponding time data were saved for each pulse from the entire input file, the output files could be populated. The files were again formatted, as seen in table 5. Each output file length was set to only encompass 8192 pulse and time pairs as this would allow for these CSV files to

be opened in excel and every pulse observed. This resulted in many output files (around 200) but was necessary as excel only extended the visible columns out to 16,384.

V.B.1. Process the Compass Raw Pulse Data Into a Useful Format for the Further Analysis.

In Python, a "Time response" script was created in Neutron Sensing Laboratory by Xiaodong Tang to plot all the corrected pulse data as shown in Appendix A. In Figure 22, the x-axis presents the time (ns), the left y-axis presents the voltage with unit mV, and the right y-axis presents the ADC unit. There were several properties that were used in the code to help us to observe the pulses better. Firstly, since we knew each correct CSV file length was limited to 8192 pulses, it could allow the researcher to see all the pulses corresponding to their time. When the researcher tried to fit the exponential curve and determine the fast and slow components, it would help find any pulse and time pairs from the CSV file. Before the algorithm of python fitting the exponential script was created, the pulses data and corresponding time pairs were plotted in excel to determine the mean decay time for the fast and slow components. Even though the excel fitting the quantification limitation, researchers could compare results from two methods and avoid significant errors.

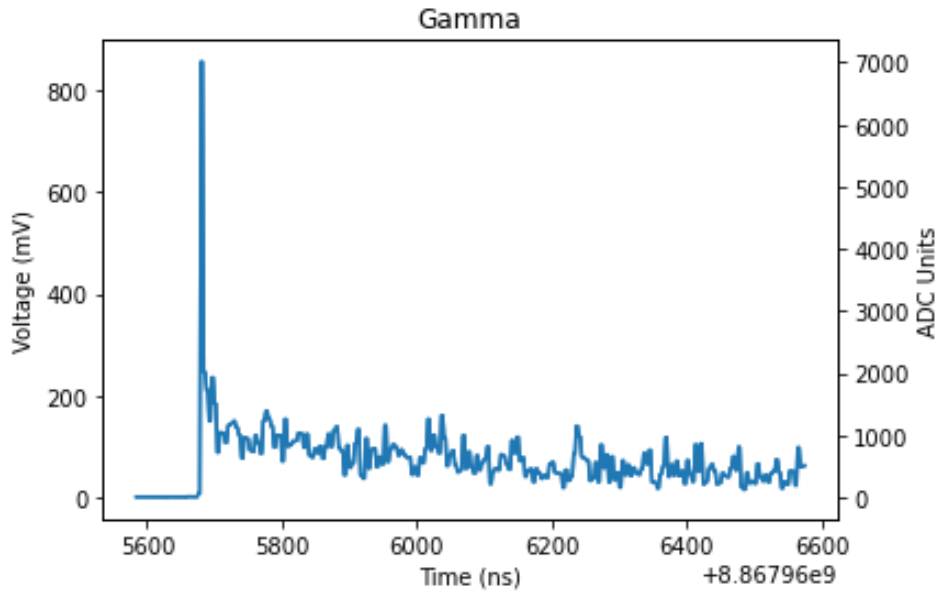

Figure 22. One example of "Time responses" python script was plotted when the maximum height pulse was set to 500mV.

However, if the researcher was trying to analyze more pulses such as 50,000 instead of 8,192, this change to the number of pulses was carried out in Python. In order to observe the clean pulses, the variable of maximum pulse height was set up to property values such as 96, 350, and 500 mV. In Figure 22, minimum pulse height was limited to 500 mV. Another characteristic of Python script that must be discussed is the number of pulses discriminated against. When the variable of the number of discriminated pulses was set to 10, it meant that the first ten pulses which satisfied the condition were plotted. The number of discriminated pulse values was proportional to the pulse minimum height value. When the minimum height value (threshold) was lowered, more pulses met the condition and were plotted.

For this step, the data in each CSV file needed to be analyzed separately. Instead of combining all file data into a single large numpy array as previously done, the files were defined

one by one. This was carried out by using the "len ()" function to define the range of pulses that would be extracted from the files to be equal to the length of one individual file (50,000 pulses). Because Python begins counting at 0, while the pulses begin their numbering at 1, the length value was added by one throughout such that the right pulse data could be extracted. So, the script counted from pulse 1 to pulse 50,000. This process was repeated for each CSV file, and the numbers deciding which file to extract data from had to be saved in active memory.

V.B.2. Fit the Exponentials Curve to the Fast and Slow Components of the Detected Pulses.

Following the raw pulse data output by CoMPASS, a python algorithm was developed. The raw data was formatted with individual points of each pulse in ADC units with an accompanying timetag. Using the timetag, a range of times corresponding to each point was created. Each pulse data point was flipped over the x-axis (time axis), corrected up to a positive scale by adding the set baseline parameter, and then the unit converted from ADC to mV. This created lists of pulses in mV per time (ns), from which the pulse heights and times were extracted. These BaF_2 pulses consist of a slow and fast component which can be represented by the formula:

$$P(t) = Ae^{-\lambda_1 t} + Be^{-\lambda_2 t} \qquad \text{Eq. (11)}$$

where P is the pulse values, A and B are the amplitudes of the fit line, t is the time in nanoseconds, λ_1 is the fast component, and λ_2 is the slow component. The constants λ_1 and λ_2 are equal to 1 over the fast time and slow time responses, respectively. They were compared to the general value expected for the fast and slow time components of ^{137}Cs. To get a statistically significant value of λ, around 200 individual pulses must be fitted. Using a signal generator

(function generator), the time response of each pulse will be calculated. Fake signals (pulses) will be generated through a digitizer connection such that a time response can be extracted. This process will also determine the value if there is a dead time occur.

VI. EXPERIMENTAL RESULT AND ANALYSIS

VI.A.1. The BaF_2 Energy Calibration using ^{137}Cs and ^{60}Co Source.

The BaF_2 scintillation detector was borrowed from the Sherry Yennello research group of the Cyclotron Institute at Texas A&M University. The radioactive sources ^{137}Cs and ^{60}Co were used for energy calibration before each measurement. The ^{137}Cs source could be utilized as a power history-resistant burn-up indicator, so it was used for the real measurement. The gamma-ray energy spectrum of BaF_2 showed a 661.7keV photopeak of ^{137}Cs with different high voltages from 2.0 to 2.4 kV. The best energy resolution of BaF2 was explored and found to be 16.6%, with a corresponding high voltage of 2.1kV.

The spectroscopy distribution for the energy calibration confirmation can be seen in Figure 23. This figure was the result of a 5-minute count of ^{60}Co and ^{137}Cs. It displayed various peaks which correspond to the photopeak of ^{60}Co and ^{137}Cs. The first clear peak showed a photopeak of ^{137}Cs, located at .6617 MeV. The second peak, seen as wider than the one for ^{137}Cs, was the combination of both photopeak for ^{60}Co. These photopeak correspond to 1.173 MeV and 1.332 MeV. The energy distribution shown in Figure 23 had not been corrected for background, as it was merely being used for calibration. It should be noted that for further data analysis, all data used was corrected for background.

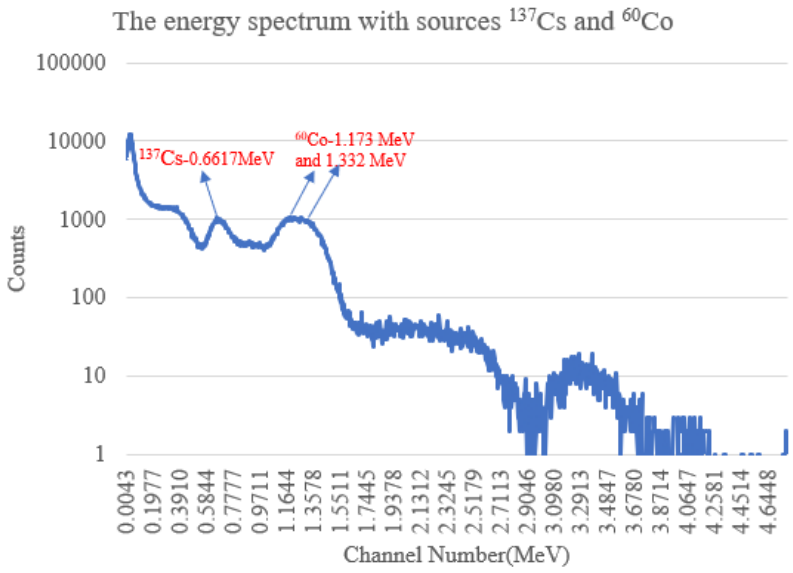

Figure 23. The energy spectrum (counts per energy channel) with sources ^{60}Co and ^{137}Cs present, as detected by a BaF_2 detector and using CAEN CoMPASS Software for data acquisition.

VI.A.2. The Optimum Energy Resolution for the BaF_2 Detector was Determined it.

Table 6. The recorded photopeak, channel number, and energy channel number along with calculated FWHM, energy resolution and error preparation for each high voltage tested.

High Voltage (kV)	Photopeak (Counts)	Channel (keV)	FWHM	Energy Resolution (%)	Channel (ADC)
2.0	14084	661.7	130	19.65	156
2.1	**14285**	**661.7**	**110 ± 6.83**	**16.62 ± 1.03**	**230**
2.2	9353	661.7	124	18.74	331
2.3	5236	661.7	124	18.74	476
2.4	2953	661.7	130	19.65	656

Table 6 displayed the investigation results to determine the best energy resolution and high voltage for the BaF_2 detector. It shows the recorded values for each high voltage that was investigated. From Table 6, it was cleared that the best high voltage to use was 2.1 kV, as it corresponded to the lowest energy resolution percentage. This line of data was highlighted in bold, and the high voltage of 2.1 kV was used moving forward from this point of analysis. Each line of data corresponds to a 20-minute run with a ^{137}Cs source that has been corrected with a 20-minute background run. The detector was already calibrated for these runs as can be seen in the energy channel column recorded.

VI.A.3. The Uncertainty Analysis Included Systematic and Stochastic Errors.

Error propagation was used to deal with uncertainties based on a large collection of numbers. The manipulation of measured quantities and the error associated with each quantity will contribute to the error in the final answer. Table 6 shows the investigation results used to determine the best energy resolution and HV for BaF_2. The table includes six parameters which are HV, photopeak, energy (ADC) channel number (ADC) along with calculated FWHM and energy resolution. Since the energy channel numbers exist as the constant values along the x-axis, the energy channel (ADC) numbers are fixed. The error propagation method which is used to determine the uncertainty of the photopeak (counts) involves manipulation along the y-axis. Because the uncertainty of FWHM was determined by calculating the corresponding channel number of half of the maximum photopeak located at the x-axis, the error propagation technique was not able to calculate the uncertainties of FWHM and energy resolution. Therefore, the systematic uncertainty method was used to calculate the FWHM. Since the energy resolution was

the ratio of the FWHM and energy channel number, their relevant uncertainty was calculated. In table 6, the uncertainties of FWHM and energy resolution were calculated only for the optimal high voltage at 2.1kV.

Systematic errors are due to identified causes and can, in principle, be eliminated. Errors of this type of result in measured values that are consistently too high or consistently too low. In this paper there are a few systematic errors to be concerned with, all of which will be resolved in the future. Firstly, based on previous studies, the surface of the BaF_2 detector has been polished to achieve the best possible optical quality. In the experiment, the BaF_2 should have been wrapped with several layers of Polytetrafluoroethylene (PTEF) tape to ensure a low reflection loss at the scintillator surfaces. Secondly, lead bricks stored in the laboratory were used to shield the radioactive source and were placed 2 cm away from the detector. This was done because the lead metal is highly effective in providing protection from sources of radiation and can be used against various high-energy applications of radiation, including gamma rays, x-rays. However, whether the lead bricks used for this experiment are irradiated or not has not been determined. There may also not have been enough bricks used to shield the BaF_2. The shielding geometry should cover all of the detector because the sensitive part of the detector is the entire crystal which is the entire hexagonal region. Shielding allows for outside radiation to be stymied such that only the applied source radiation is present in the counts. This result is usually not completely accomplished but approaching such a goal is necessary. Geometric efficiency is known to be the biggest detractor to total efficiencies of detectors. The actual distance from source to detector was measured with a ruler to be 2 cm, which with basic uncertainty principles

has an error of 0.05 cm. However, the systematic uncertainty in the position does not contribute to the energy resolution determination.

VI.A.4. Gamma-Rays Energy Spectrum of the Pebble Bed Were Broadened by MATLAB.

Since the digitizer used (DT5730), the analog to digital conversion has 16,384 energy channels corresponding to the counts, all peak counts corresponding to 16,384 energy bins were broadened to Gaussian pule and eventually summed up. Figure 24 shows the gamma-ray spectrum of BaF_2 with an Energy Resolution of 15% after broadening the energy peaks. The x-axis was presented as the energy deposited (MeV), and the y-axis was presented as the counts. The spectrum used is from Xenon-100 provided by X-Energy LLC. The broadened nature of the spectrum allows for more clearer peaks and valleys. Without this, the spectrum in its entirety would be much like what is seen in Figure 24 for energies below 0.1 MeV.

Even though the BaF_2 is one of the fastest scintillation detectors, it has its drawbacks. All the broadened energy peaks from hundreds of fission products of a pebble burned to 160 GWd/MTU, are reduced to only a few gamma-ray energies in Figure 24. There are only few fission products were identified, and the isotopes with their half-lives and photopeak showed in table 7. When trying to perform security studies, the inspector looks at gamma-ray lines to tell which fission products are there, and then they can tell what the burn-up is, and burn-up can tell how much plutonium is. Now, if an inspector is trying to do gamma-ray spectroscopy, that measurement would measure very few gamma-ray lines with BaF_2. Thus, the determination of burn-up could be a challenge.

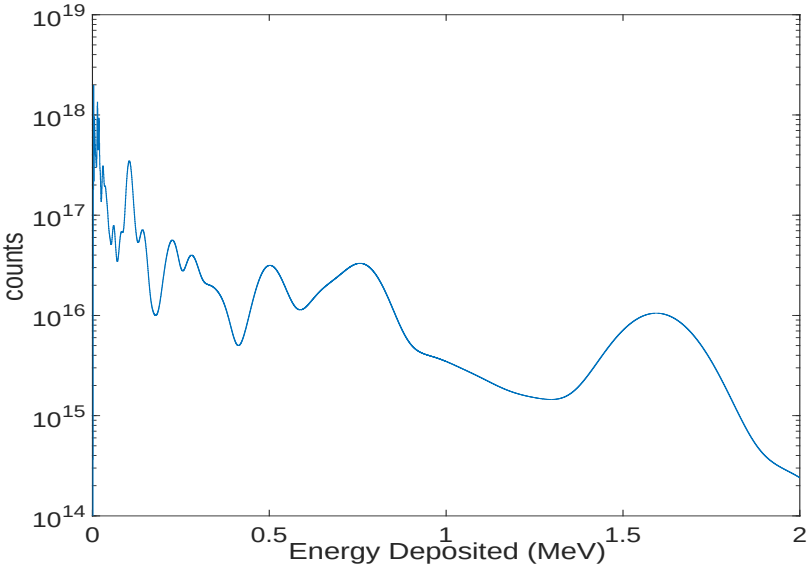

Figure 24. Pebble-Bed Reactor gamma-ray spectrum after broadening the energy peaks of BaF_2 energy resolution.

Table 7. The identified isotope from BaF_2 with 15% energy resolution

Isotopes	Photopeak (keV)	Half-life
^{132}Te	230	77 hours
^{155}Eu	105	4.76 years
^{103}Ru	497	38.26 days
^{95}Zr	756	65 days
^{140}La	1596	40 hours

Therefore, Figure 25 shows the pebble-bed reactor gamma-ray spectrum after broadening the energy peaks of HPGe with an energy resolution of 0.3% of the BaF_2 energy spectrum. Also, fission fragments with their half-lives and photopeak showed in table 8 as well. Both broadening gamma-ray spectra were using the same data. In addition, Figure 25 shows the spectrum of

energies emitted by the source using the HPGe detector. Comparison of the peaks found in a spectrum against a library of known radionuclides energies and abundance allows identification of components of a sample. Comparing different detectors with their energy resolution, the HPGe offers better energy resolution and is a good instrument for unambiguous nuclide identification compared with the BaF_2 detector. Also, the HPGe detector provides the advantage of resolving two closely located energy points and has the ability to detect a mixture of nuclear material.

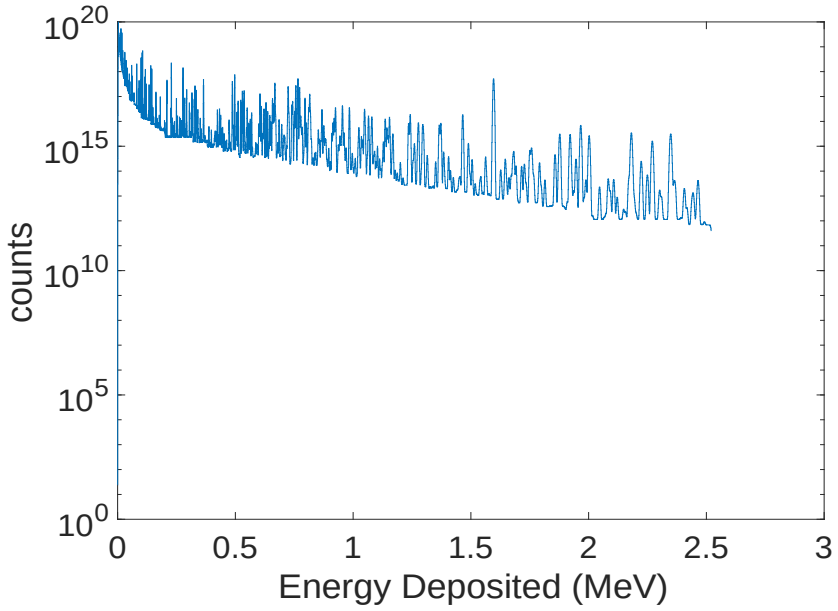

Figure 25. Pebble-Bed Reactor gamma-ray spectrum after broadening the energy peaks of HPGe energy resolution.

Table 8. The identified isotope from HPGe with 0.3% energy resolution

Isotopes	Photopeak (keV)	Half-life
^{22}Na	511	2.60 years
^{137}Cs	661.7	30.2 years
^{152}Eu	1408	12 years
^{40}K	1460	$1.29*10^{9}$ years
^{140}La	1596	40 hours
⋮	⋮	⋮

VI.A.5. Burnup Determination Analysis

A nuclear fission reaction occurs when a neutron is absorbed by a ^{235}U nucleus, changing the ^{235}U atom to an excited state which causes it to split into two smaller fission fragments. The fission process can often produce more than one neutron which is then absorbed, maintaining the fission chain reaction and releasing both 200 MeV energy and gamma photons as shown as Eq.12.

$$U^{235} + n \rightarrow U^{236} \rightarrow Xe^{140} + Sr^{94} + 2n + 200\ MeV \qquad \text{Eq (12)}$$

When a ^{235}U atom undergoes fission, the two most probable primary fission fragments produced are xenon and strontium. The atomic numbers of xenon and strontium are 140 and 94 respectively. ^{140}Xe, which has a highly radioactive fission fragment, decays quickly due to its 14 second half life from a very unstable state to the stable isotope ^{140}Ce. The other common fragment ^{94}Sr, with a 75 second half-life, decays to the stable isotope ^{94}Zr. Figure 26 shows the

percent yield of fission fragments as a function of atomic mass A. Most of the fission fragments are located around atomic numbers 94 and 140, with the average being 118. These distributions of mass numbers surround exactly what would be expected considering the two primary fission fragments produced, xenon and strontium.

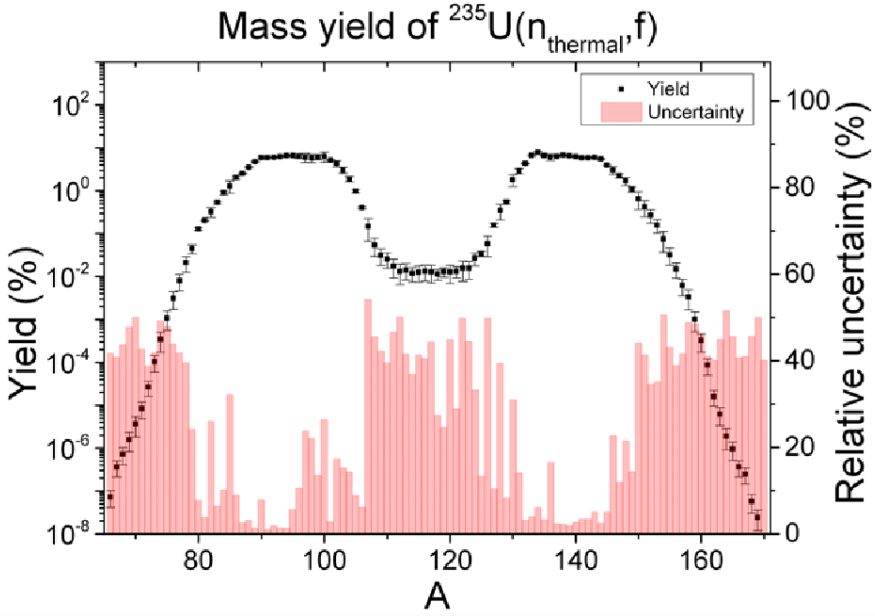

Figure 26. The ^{235}U percent yield of fission fragments as function of atomic mass A. Reprint from [Pomp, Stephan et al. "Accurate FissiOn data for Nuclear Safety (AlFONS) : Final Report." (2015).]

An inevitable byproduct of nuclear fission is the production of fission products which are highly radioactive. ^{137}Cs is one of the most dangerous radioisotopes to the environment in terms of their long-term effects. The decay scheme of ^{137}Cs can be seen in Figure 27. The half-life of ^{137}Cs is known to be about 30.17 years, and around 94.6% of it decays to ^{137m}Ba through beta ray emission. Another 5.4% directly decays to the ground state of ^{137}Ba. The metastable ^{137m}Ba itself decays to the ground state by emission of a 661.7 keV gamma-ray. A total 85.1% of ^{137}Cs decays will lead to gamma-ray emission. This produces a gamma spectrum which shows a good

resolution peak. The important characteristics of ^{137}Cs are that it is only highly radioactive, but instead, it has a long enough half-life to be around for hundreds of years emitting radiation. ^{137}Cs is also known to has an extremely small absorption cross-section 0.253b. (1barn = 10^{-24} cm^2)

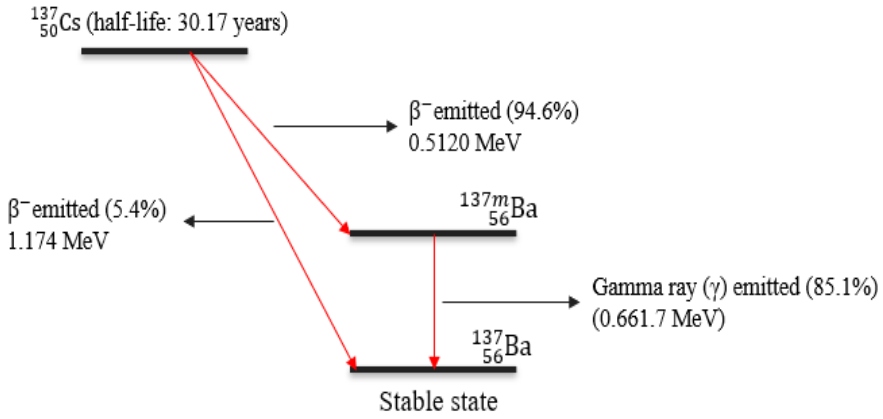

Figure 27. The decay scheme of isotope ^{137}Cs.

In nuclear physics, burnup is defined by the amount of energy extracted from the primary nuclear fuel. Its units are gigawatt-days/metric tons (GWd/tHM) of heavy metal. Because of the previously discussed characteristics, ^{137}Cs as one of most important isotopes used in determining the reactor fuel burnup among all of the non-destructive spectrometric methods. The inventory of ^{137}Cs along the fuel rods is proportional to the local burnup. Gamma spectrometry is a non-destructive, rapid, and low-cost method that serves to determine the activity of all emitting fission products still present in a fuel rod at the time of measurement.

An example of the ^{137}Cs decay dynamic is displayed in Eq 13. The inventory of the ^{137}Cs is equal to amount of the ^{137}Cs which are produced by fission reaction subtract absorption and decay of the ^{137}C, since the ^{137}Cs fission yield (Ycs137) is 6.9 %.

$$\frac{\mathrm{dN}}{\mathrm{dt}} = \text{prodction} - \text{decay} - \text{abosoprtion}$$

$$\frac{dN}{dt} = N_{U235}\sigma_f \phi Y_{cs137} - \lambda_{cs137}N_{cs137} - N_{cs137}\sigma_{absorption}\phi \qquad Eq.13$$

Where:

N: The atom number density (atoms/cm^3)

σ_f: The fission microscopic cross section (cm^2)

ϕ: neutron flux (neutron/cm^2.s)

λ_{cs137} = decay constant of the ^{137}Cs (s^{-1})

$\sigma_{absorption}$= The gamma ray absorption cross section (cm)

Y_{cs137} = ^{137}Cs fission yield (%)

$$\frac{dN}{dt} = N_{U235}\sigma_f \phi Y_{cs137} \qquad Eq.14$$

Recalling the characteristics of ^{137}Cs, the decay and absorption sections can be ignored due to the long half-life and sufficiently small absorption cross section. Eq.13 can be converted to Eq.14.

$$N = N_0 + kt \text{ (Linear)}$$

$$\left(k = \ constant = N_{U235}\sigma_f \phi Y_{cs137}\right) \qquad Eq.15$$

In the Eq. 16, the left-hand side parameters are not as function of time, so it is assumed that k is constant. After that, the Eq.14 combines with the constant coefficient equations which results in Eq.15. Figure 28 showed the linear plot of the inventory of ^{137}Cs as function of the Burnup. In this research, since the energy resolutions of BaF_2 and HPGe are 15% and 0.3%, the gamma-ray energy spectrum of the pebble bed was broadened with two energy resolutions. From

Figure 25, we can identify many isotopes by using the HPGe rather than the BaF_2 because the HPGe has a much better energy resolution. However, there are only a few isotopes able to be identified and some of them are overlapped within one wide pulse. When an HPGe scintillation detector was used to detect a pebble, taken from the reactor after cooling 90 hours, the burnup was determined using the ^{137}Cs as the burnup indicator. This was possible because the ^{137}Cs photopeak was clearly identifiable from the gamma-ray energy spectrum as shown in Figure 25. Eq 16 is the single fission product gamma-ray activity equation. From Eq.16, the $C^{'}$ represents the count rate, ε represents the efficiency of the detector, P_B represents the branching ratio of the gamma, S_{atten} represents the surface attenuation of the material, λ represents the decay constant, and $e^{-\lambda t}$ represents the cooling time. In Eq 16, the only unknown parameter is N_{fp} which represents the atom density of the fission product. Since we determined the N_{fp}, we could determine the single burnup yield by using Eq 17. Consequently, we were able to plug in both of those calculated values to compared with the linearity of the ^{137}Cs burnup as a function of the mass in Figure 28. This finally determined the burnup of each pebble. As a result, we could identify which pebble is to recirculate, and which one needs be replaced by new fuel.

$$C' = \varepsilon\ P_B\ S_{atten}\ N_{fp}\ \lambda\ e^{-\lambda t} \qquad Eq.16$$

$$BU(atom\ \%) = 100\ \frac{N_{fp}}{Y_{fp}\ N_U} \qquad Eq.17$$

In Figure 24, we cannot determine the burnup by using ^{137}Cs. Another photopeak isotope, with an individual photopeak and the ability to do the burnup determination, must be picked. This is the reason why burnup determination can be a challenge.

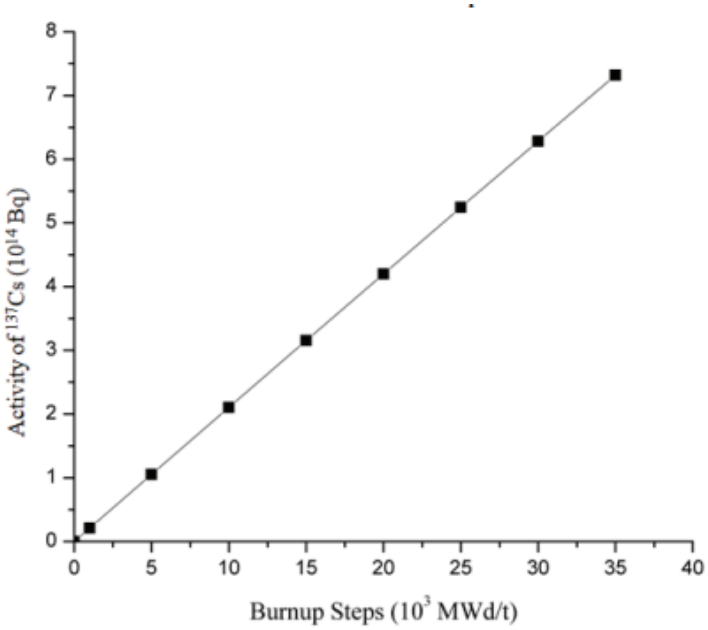

Figure 28. The inventory of the ^{137}Cs in the fission reaction as function of the Burnup. Reprint from [S.N. Inayah, Suharyana, Riyatun, and A.Khakim "Calculation of ^{134}Cs, ^{137}Cs, and ^{154}Eu activity as the high temperature engineering test reactor (HTTR) burn-up parameter using Monte Carlo vector processor (MVP)", AIP Conference Proceedings 2014, 020058 (2018)]

VI.B. Through Fit the Exponentials Curve to the Fast and Slow Components Of The Detected Pulses, the Mean Decay Time of Fast and Slow Components were Determined by Python Algorithm

Using the pulse-shape discrimination with BaF_2, we were able to discriminate the charged particles from neutral particles which are included gamma-ray (fast component) and neutrons (slow component). To explore the time resolution of BaF_2, a python function developed in the Neutron Sensing Laboratory by researchers Xiaodong Tang and Benjamin Wellons. It was used to process the collected data, fit various pulses to the exponential curve, and determine the fast and slow components of BaF_2. Then the fast component curve was separated to investigate the rising time and time characteristics of BaF_2.

The fast and slow components could be seen in the left image of Figure 29. After reaching the pulse height there was a sharp drop in voltage over time followed by a slower drop in voltage on time. These two distinctly different slopes could be observed in the left image of figure 29. The two components were what was used to fit Eq. (11) to and solved for the values of λ_1 and λ_2. This process was done for over 200 pulses to extract a statistically significant average. The pulses used for the exponential fit were discriminated to be only those above 350 mV pulse height. Such discrimination was required to eliminate pulses that did not have a clean enough distribution to be properly analyzed and fitted. An example of one of these pulses is shown on the right side of figure 29. This pulse could be seen to not involve a distinct fast or slow component, as after the pulse reaches its peak the values proceed to vary wildly. After analyzing such poor quality "noise" pulses, a desired minimum pulse height of 350 mV was determined. The implementation of this discrimination resulted in around 200 "clean" pulses. These pulses were then used in the exponential fit outlined above. It is assumed that the "noise" pulses as shown on the right side of figure 29 were the result of electronic noise in the BaF_2 detector and digitizer configuration.

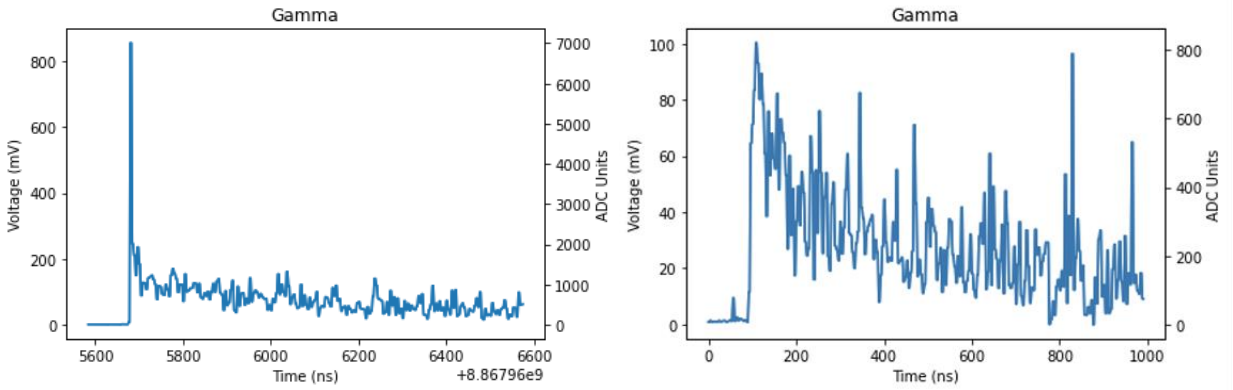

Figure 29. An example "clean" gamma pulse from ^{137}Cs source detected by BaF_2 detector (left) and an example "noise" gamma pulse from ^{137}Cs source (right).

An example of the resulting exponential fits to the pulses could be observed in figure 30. In the top left, one can see the initial raw pulse data separated into the fast and slow components. These components were used to create two exponential fit lines shown in the top right of figure 30. The direct comparison of each fit to its respective component was shown in the bottom right and bottom left of figure 30. From these fits, the mean decay time could be calculated being $1/\lambda_1$ and $1/\lambda_2$ for fast and slow components, respectively. These fast and slow responses along with other relevant data were found in Table 9 below. This calculation was conducted in Python code as the exponential fit and subsequent plots were created. The specific python function used to fit the data was "MonoExpZeroB (x, m, t)" where x represented the time component (T), m represented the amplitudes A and B, and t represented the fast and slow time components λ_1 and λ_2.[8]

The process of exponentially fitting a curve to the data in python required importing SciPy. To fit the curve, you need to define it as a function. Then calling scipy.optimize.curve_fit will tweak input starting values to best fit the data. In this instance it is known that the data should be decaying to 0, as that will be acting as the baseline of the pulse. Because of this the usual function of monoExp (x, m, t, b) is redefined as monoExpZeroB (x, m, t). This change simply removed the constant b, which defined what value on the y axis the exponential decayed to. It's important to note that this method only works for a singular exponential function, hence the "mono" term. This was rectified by simply separating the fast and slow components of each pulse so that they could be individually fitted before then combining each fit on the same plot. This is easily shown in figure 30.

The specific Python code was developed in Neutron Sensing Laboratory by Xiaodong Tang. In the script the data is first imported and separated into pulse and time numpy arrays. Then the pulses were filtered based on their heights such that no pulses under the height of 350 mV would be used in the exponential fit. This was decided in order to increase the accuracy of the fit as it was known that lower voltage pulses had a high likelihood of being simply noise. In order to get a proper average for the fit data of each pulse, each pulse had to be normalized. This was done by dividing each selected pulse by its max pulse height and then making the pulse height the start of the time axis such that every pulse would start from (0,1) where the x axis was time and the y axis a unitless ratio. From here the exponential fitting would only concern itself with rate and shape at which the data decreased down to 0 on the y axis. Such a limiting of parameters would allow for the decay constants to be far more relevantly accurate. Once the function was defined, the fast and slow components of the pulses were split into separate arrays. After analyzing many pulses in the data, it was determined that the fast component ended after just 4 data points (2 unique sample points) while the slow component extended on for some time. Because of this the fast component was selected to be those first 4 data points after maximum pulse height while the slow component was estimated to extend 95 more sample points after the end of the fast component.

Now the most important part of the fitting comes from the function scipy.optimize.curve_fit (f, xdata, ydata) which uses non-linear least squares to fit a function, f, to the data inputted. The model function f must take the independent variable as its first argument. The xdata and ydata are understandably just the time data and the pulse data for each component (fast and slow).

Finally, there is another input to the function, p0, which is the initial guess for the parameters A, B, 1, and 2 as seen in Eq. (11).

In the script the initial guess parameters are first defined. For the fast component they are selected to be A = 1 and 1= 1.25. It is known in this case that the value of A will be 1, as the curve starts from 1 on the y axis, however the value of 1 is simply a guess from understanding what the typical values should be. For the slow component B = 0.2 and 2= 0.00159. Again the 2 value is determined the same but in this case the value of B is simply estimated by looking at where the slow component typically starts on the y axis. It is known that the fast and slow time responses are known to be Eq. (11) over their respective components (1 and 2), so their values are calculated along with the component's values. The values of A and B will be calculated as well but are less relevant. Once the curve_fit function has done its job a time array is created for the length of all the pulse data and plugged into the monoExpZeroB function along with the other parameters. Plots are created to represent the journey of creating each exponential fit and one pulses example of this is seen in figure 30. The values of the fast and slow components are also saved into numpy arrays. These arrays are then averaged using the "np. Mean" function imported with NumPy. The mean value is then displayed allowing for its extraction. The culmination of these responses along with their theoretical values and error differences is shown in Table 9.

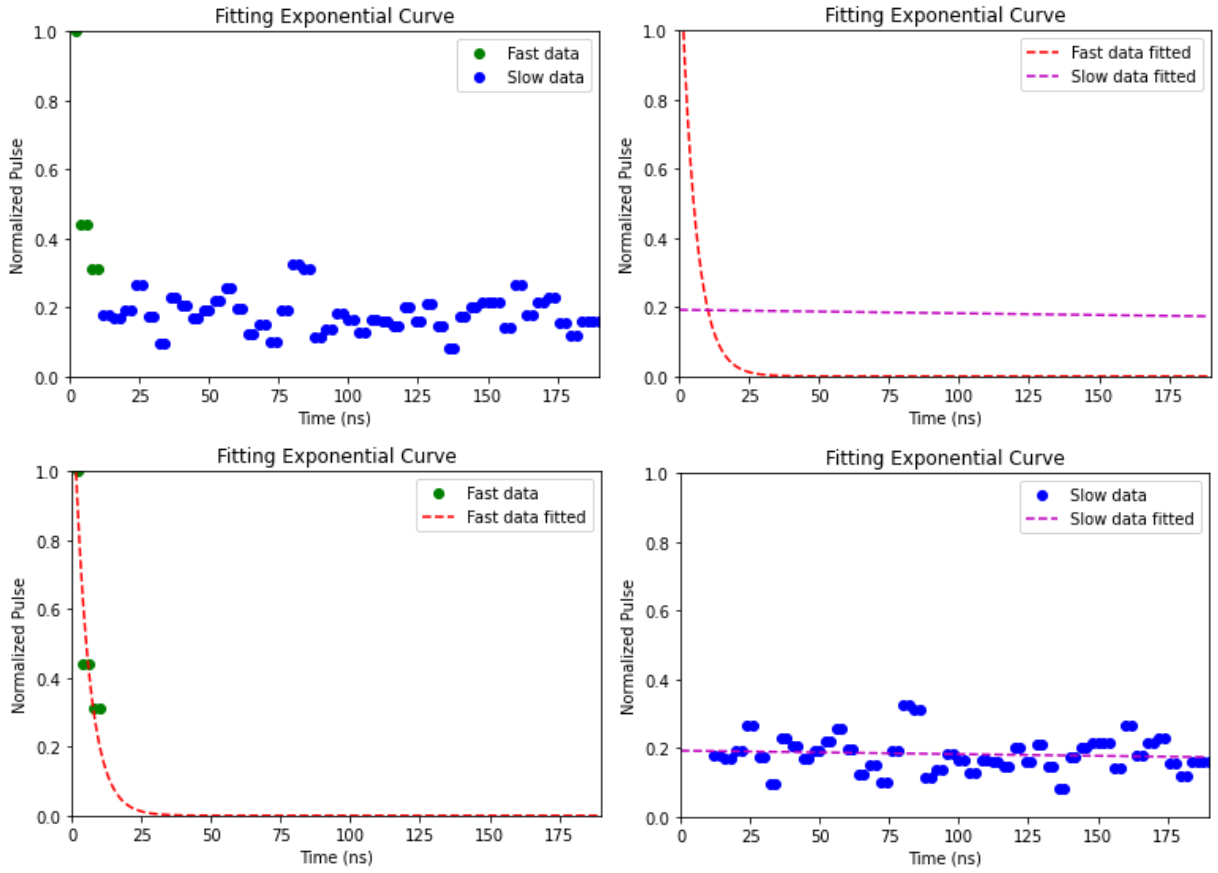

Figure 30. Data points for the fast and slow components of a pulse (top left), exponential fit lines for the fast and slow components of that pulse (top right), exponential fit line and data points for fast component of that pulse (bottom left), and exponential fit line and data points for the slow component of that pulse (bottom right).

Table 9. The fast and slow components of both the experimental and theoretical data along with the percent differences.

	Fast Response (ns)	Slow Response (ns)
Experimental Data	0.99	648
Theoretical Data	0.80	630
Error Different (%)	12.50	2.85

The fast and slow components of both the experimental and theoretical data along with the error difference (%) between the two, are shown in Table 9. Theoretically, the fast and slow time responses of the BaF_2 detector are 0.8 ns and 630 ns, respectively.[2] These theoretical values

were compared with the experimental data, and the error difference between them was calculated. The result shown was that the slow response (2.85%) has a better agreement than the fast response (12.5 %). This is because, due to a poor time resolution of the fast response, only five data points of the fast response were collected by the detector meaning the exponential fit was less statistically accurate. A CAEN's 500MHz digitizer was used to collect the data at a rate of one data point for every 2 or 4 nanoseconds. Instead of using this 500MHz digitizer, a faster digitizer with 1 or 4 GHz could be used to collect more data. Consequently, with such a faster digitizer and data acquisition system, the results could be made more statistically accurate.

VII. CONCLUSIONS

In this experiment, the goal was to be measure and analyze the energy and timing characteristics of the BaF_2 scintillation detector. The detector was used to explore the energy resolution characterization for gamma-spectroscopy, including high voltage determination, energy calibration, and the optimum energy resolution of the BaF_2 detector. The radioactive sources ^{137}Cs and ^{60}Co were used for energy calibration before each measurement. After that, the FWHM was determined, and then the best energy resolution of BaF_2 was explored and found to be $16.62 \pm 1.03\%$ with a corresponding high voltage of 2.1kV.

Secondly, the time resolution of the BaF_2 detector was explored through measurements and fitting exponentials. The mean decay time of the fast and slow components were explored by fitting exponentials to them using a Python function. Experimentally, the fast response and slow responses were equal to 0.99 and 648 ns. Comparing the theoretical data and results, the slow response component (2.85%) has a better agreement than the fast response (12.5 %). This is due to a poor time resolution of the fast response, with only five data points of the fast response being collected by the detector, meaning the exponential fit was less statistically accurate. There was a total of 200 pulses used to calculate the fast and slow response time.

Finally, MATLAB was assigned to broaden the gamma-rays energy spectrum of the pebble bed reactor. The 16,384 energy channels were broadened with different energy resolution data including HPGe (0.03%) and BaF_2 (15%). After comparing the two detectors using their energy resolution, the HPGe offered better energy resolution and was a good instrument for unambiguous nuclide identification compared to BaF_2 detector. For instance, when trying to

perform security studies, an inspector analyzing the gamma-ray lines could determine which fission products are present and thus the burnup/enrichment could be determined. For this inspector performing, gamma-ray spectroscopy, a measurement with BaF_2 would measure very few gamma-ray lines. Thus, the determination of burn-up or enrichment could be a challenge.

VII.A Future Steps

In the future, the time component of the two exponential fits will be used as an approximation of over 1000 pulses, instead of just 200 pulses, to get a statistically significant average. This process will be done with Python code developed here. The impact on material balance accounting will also be explored. It will be determined how this system affects the inventory of ^{239}Pu and ^{235}U at a reactor site. Additionally, this work will help in developing a design for an extremely fast detection system capable of performing on-the-fly pulse analysis.

REFERENCES

1. Chen, Hawari, A. I. (2007). Nuclear Instruments and Methods in Physics Research Section A: Accelerators, Spectrometers, Detectors and Associated Equipment. *Analysis of the Impact of Random Summing on Passive Assay of Pebble Bed Reactor Fuel Using Gamma-Ray Spectrometry*, *579*(1), 297–300. https://www.sciencedirect.com/science/article/pii/S016890020700633X
2. CRYSTAL SAINT-GOBAIN. (n.d.). *BaF2 Barium Fluoride Scintillation Material*. Www.Crystals.Saint-Gobain.Com. Retrieved April 15, 2021, from https://www.crystals.saintgobain.com/sites/imdf.crystals.com/files/documents/barium-fluoride-data-sheet.pdf
3. Cyclotron Institute at Texas A&M University. (n.d.). *Use of the ORNL-MSU-TAMU BaF2 Array by Robert Varner*. SJY Group Cyclotron Institute at Texas A&M University. Retrieved April 15, 2021, from https://cyclotron.tamu.edu/sjygroup/baf2-array/
4. Heinz Nabielek, Malin Liu, Bing Liu,. (2020). Nuclear Engineering and Design,. *Burn-up Measurement Error Analysis of HTR Fuel Spheres Using Ab-Initio Monte-Carlo Simulations*, *363*, NA. https://www.sciencedirect.com/science/article/pii/S0029549320301254
5. Jianwei Chen, Ayman I. Hawari, Zhongxiang Zhao, Bingjing Su,. (2003). Nuclear Instruments and Methods in Physics Research Section A: Accelerators, Spectrometers, Detectors and Associated Equipment, *Gamma-Ray Spectrometry Analysis of Pebble Bed Reactor Fuel Using Monte Carlo Simulations*, *505*(1–2), 393–396. https://www.sciencedirect.com/science/article/pii/S0168900203011057

6. Ulrich Ackermann, Werner Egger, Peter Sperr, Günther Dollinger. (2015, June 21). Nuclear Instruments and Methods in Physics Research Section A: Accelerators, Spectrometers, Detectors and Associated Equipment. *Time- and Energy-Resolution Measurements of BaF2, BC-418, LYSO and CeBr3 Scintillators*, *786*(0168–9002), 5–11. https://www.sciencedirect.com/science/article/pii/S0168900215003101
7. CAEN S.p.A. (2010). *DT5730 / DT5730S - 8 Channel 14 bit 500 MS/s Digitizer*. CAEN - Tools for Discovery. https://www.caen.it/products/dt5730/
8. *Exponential Fit with Python*. (2020, September 24). SWHarden.Com (The Personal Website of Scott W Harden). https://swharden.com/blog/2020-09-24-python-exponential-fit/
9. *Sampling Speed Details | spectrum*. (2019). SPECTRUM. https://spectrum-instrumentation.com/en/sampling-speed-details
10. Hossaln, I., Sharip, N., & Viswanathan, K. K. (2012). Efficiency and resolution of HPGe and NaI(Tl) detectors using gamma-ray spectroscopy. *2012 Academic Journals*, *7（1）*(1992–2248), 86–89. https://academicjournals.org/journal/SRE/article-full-text-pdf/8190CA926783
11. The OHIO STATE UNIVERSITY. (2021). *Gamma-Ray Spectroscopy*. Nuclear Reactor Laboratory. https://reactor.osu.edu/gamma-ray-spectroscopy
12. X. Grinstead, Charles M.; Snell, J. Laurie (2009). "Conditional Probability - Discrete Conditional" (PDF). *Grinstead & Snell's Introduction to Probability*. Orange Grove Texts. ISBN 161610046X.
13. Eckert and Ziegler Isotope Products, Inc. manufactures, distributes, and supplies radioactive sources 24937 Avenue Tibbitts, Valencia, CA 91355 (USA) (www.isotopeproducts.com).
14. Gilmore G, Hemingway JD (1995). Practical Gamma-Ray spectrometry (New York: Wiley)

15. Hult M (2007). Low-level gamma-ray spectrometry using Ge-detectors. IOP publishing Metrologia 44: S87-S94.
16. Knoll GF (1989). Radiation Detection and Measurements (New York: Wiley
17. Metzger RL, Van Riper KA, kearfott KJ (2002). "Radionuclide depth distribution by collimated Spectroscopy" ANS Topical Meeting, Santa Fe, NM.
18. W.E.U.A.P.S.G.D. (2015b). Time- and energy-resolution measurements of BaF2, BC-418, LYSO and CeBr3 scintillators. *Nuclear Instruments and Methods in Physics Research Section A: Accelerators, Spectrometers, Detectors and Associated Equipment*, *786*(0168–9002), 5–11. https://www.sciencedirect.com/science/article/pii/S0168900215003101#s0030
19. H.N.M.L.B.L. (2020). Burnup measurement error analysis of HTR fuel spheres using ab-initio Monte-Carlo simulations, *Nuclear Engineering and Design*, *363*(0029–5493). https://www.sciencedirect.com/science/article/pii/S0029549320301254
20. Med Phys. (n.d.). *Radioisotopes and Radiation Methodology*. Scintillation Detectors. Retrieved July 30, 2021, from https://www.science.mcmaster.ca/radgrad/images/6R06CourseResources/4R6Notes4_ScintillationDetectors.pdf
21. Wikipedia contributors. (2020, December 29). *Scintillation counter*. Wikipedia. https://en.wikipedia.org/wiki/Scintillation_counter
22. KNOLL, K. (2021). *Radiation Detection & Measurement (3rd, 00) by Knoll, Glenn F [Hardcover (2000)]* (3rd ed.). Wiley, Hardcover(2000).
23. *Photomultiplier - an overview | ScienceDirect Topics*. (2011). Photomultiplier. https://www.sciencedirect.com/topics/medicine-and-dentistry/photomultiplier

24. Wikipedia contributors. (2001, November 10). *Gamma ray*. Wikipedia. https://en.wikipedia.org/wiki/Gamma_ray#:%7E:text=In%201903%2C%20Ernest%20Rutherford%20named,ascending%20order%20of%20penetrating%20power.

25. *Photoelectric effect*. (07–08-05). Wikimedia Commons. https://commons.wikimedia.org/wiki/File:Photoelectric_effect.svg

26. *Pair Production and Annihilation - MSE 5317*. (n.d.). Wikidot. Retrieved July 30, 2021, from http://electrons.wikidot.com/pair-production-and-annihilation

27. COMPTON, A. H. (1923). Recoil of Electrons from Scattered X-Rays. *Nature*, *112*(2812), 435. https://doi.org/10.1038/112435a0

28. Parks, D. J. E. (2015). The Compton Effect-- Compton Scattering and Gamma Ray Spectroscopy. *NA*, *37996*(1200). http://www.phys.utk.edu/labs/modphys/Compton%20Scattering%20Experiment.pdf

29. *GAMMA-RAY SPECTRA*. (n.d.). Faraday.Physics. Retrieved July 30, 2021, from https://faraday.physics.utoronto.ca/IYearLab/gammaray.pdf

30. *BaF2 - Barium Fluoride Scintillator Crystal*. (n.d.). Advatech. Retrieved July 30, 2021, from https://www.advatech-uk.co.uk/baf2.html

31. *NaI (Tl) Sodium Iodide Scintillation Detectors | Berkeley Nucleonics*. (n.d.). BNC Berkeley Nucleonics Corp. Retrieved July 30, 2021, from https://www.berkeleynucleonics.com/nai-sodium-iodide

32. Libretexts. (2020, August 15). *Fluorescence and Phosphorescence*. Chemistry LibreTexts. https://chem.libretexts.org/Bookshelves/Physical_and_Theoretical_Chemistry_Textbook_Ma

ps/Supplemental_Modules_(Physical_and_Theoretical_Chemistry)/Spectroscopy/Electronic_Spectroscopy/Fluorescence_and_Phosphorescence

33. Pomp, Stephan et al. “Accurate FissiOn data for Nuclear Safety (AlFONS) : Final Report.” (2015).
34. S. N. Inayah, Suharyana, Riyatun, *and* A. Khakim "Calculation of ^{134}Cs, ^{137}Cs, and ^{154}Eu activity as the high temperature engineering test reactor (HTTR) burn-up parameter using Monte Carlo vector processor (MVP)", AIP Conference Proceedings 2014, 020058 (2018) https://doi.org/10.1063/1.5054462

APPENDIX A

The Compass Pulse Data Development by using Python algorithm.

```
import csv
import matplotlib.pyplot as plt
import numpy as np
import pandas as pd
import math
from os import path
file = 'Cs137_pulse_data_25%.csv'
pulses_per_csv = 8192
## This code corrects the raw compass data files into more readable files, better units (ADC to mV), and creates a list of time data for each pulse.
num_rows = sum(1 for line in open(file)) - 1     #This part finds out the number of rows of data in the file so that arrays can be pre-allocated of that number later.
#num_rows = 30                #This part allows you to manually limit the number of rows that will be pre-allocated, use this when only looking at a set number of rows.
sample_length = 0
with open(file, newline='') as f:                #This part sets up the length of the samples, it should be 496 but this allows for if it isn't.
    csv_reader = csv.reader(f, delimiter=';')
    for counter,line in enumerate(csv_reader):
        if counter > 0:
```

```
            sample_length = len(line[4:])
        if counter > 0:             #Don't change the counter limiter in this if statement, its form only checks the length of the first row of samples to save time.
            break
##These sections pre-allocate arrays to then later fill with data edited from the csv file, this is done to save computing time.
pulses_corrected = np.zeros(shape=(num_rows, sample_length))
times_of_pulses = np.zeros(shape=(num_rows, sample_length))
#max_pulse_heights = np.zeros(num_rows)       #This would allow us to store the height of each pulse, its not necessary for tail to total.
#max_height_times = np.zeros(num_rows)        #This would allow us to store the times of the height of each pulse, its not necessary for tail to total.
##This section takes the sample data and time tags in the csv file, manipulates them, and then puts them into arrays of each pulse and their corresponding times
```

```
baseline = 0
with open(file, newline='') as f:
    csv_reader = csv.reader(f, delimiter=';')       #Opens the csv file and reads it (not the most efficient way but changing code would take too much time)
    for counter,line in enumerate(csv_reader):
        if counter > 0:
            baseline = max([int(p) for p in line[4:len(line)]])
            pulses_corrected[counter-1] = [(-float(p)+baseline) *0.1220703125 for p in line[4:len(line)]]
 #Flips pulses over x-axis, and adds baseline to pulses to correct to zero.
            max_height = max(pulses_corrected[counter-1])  #Finds the actual height of the pulses that are now corrected to be upright.
            index_of_timetag = 0
            for i,height in enumerate(pulses_corrected[counter-1]):
                if height >= .25*max_height:
#Based on CDF timetag data is recorded at (75%, 50%, or 25%) of pulse height, this finds the bin number of the timetag.
                    index_of_timetag = i
                    break
            time_list = (np.arange(-index_of_timetag+1 ,sample_length+1 - index_of_timetag, dtype=np.float64) * 2.0) + (float(line[0])/(10**3))
            times_of_pulses[counter-1] = time_list
```

```
 #Creates array of time corresponding to each pulse data point, starting from timetag bin location, and increasing/decreasing by 2ns around it.
        if counter > num_rows:  #Allows for code to read through all rows of pulse data in csv file (use to calculate tail to total of entire csv file).
        #if counter > 29:     #Limits the number of rows of pulse data that the code will read through in csv file (use for analyzing specific pulses).
            break
for i in range(math.ceil(num_rows/pulses_per_csv)):
    start_pulse = i*pulses_per_csv
    final_pulse = start_pulse + pulses_per_csv
    if num_rows < final_pulse:
        final_pulse = num_rows
    f = open(f'{file[:-4]}_CorrectedPulses{i+1}.csv', 'w')
    f.write(",".join([f"time{k+1}(ns),pulse{k+1}(mV)" for k in range(start_pulse, final_pulse)])+"\n")
    for j in range(sample_length):
        f.write(",".join([f"{times_of_pulses[k][j]},{pulses_corrected[k][j]}" for k in range(start_pulse, final_pulse)]) + "\n")
    f.close()
```

Time Response of BaF_2 determine by using Python algorithm.

```
    import csv
    import matplotlib.pyplot as plt
```

```
import numpy as np
import pandas as pd
import glob
#file = 'Cs137_pulse_data_25%_CorrectedPulses12.csv'
path = "./"
all_files = glob.glob(path+"/*.csv")
#file = []
for file_name in all_files:
    data = pd.read_csv(file_name)
    num_pulses = 50000 # How many pulses determine to investigate it(8192, 50000)
    num_discriminated_pulses = 100
    # plot first 100 that meet the satisfaction condition
    #sample_length = sum(1 for line in open(file)) - 1
    sample_length = sum(1 for line in open(file_name)) - 1
    #data = pd.read_csv(file)
    time_data = data[[f'time{i+1}(ns)' for i in range(50000*0,50000*1)]].to_numpy().T
    pulse_data = data[[f'pulse{i+1}(mV)'for i in range(50000*0,50000*1)]].to_numpy().T
    # *1,2,3,4 … present the order of files
    discriminated_time_data = np.zeros(shape=(num_discriminated_pulses, sample_length))
    discriminated_pulse_data = np.zeros(shape=(num_discriminated_pulses, sample_length))
    counter = 0
    for pulse,time in zip(pulse_data, time_data):
```

```
        index_of_max_height = 0
        max_height = max(pulse)
        for i,height in enumerate(pulse):
            if height >= max_height:
                index_of_max_height = i
                break
        if max_height >= 96
# when the pulse height was equal to 96 mV or above 96 mV, then the pulse was
    captured by the system and plot it.
            counter += 1
            discriminated_pulse_data[counter-1] = pulse
            discriminated_time_data[counter-1] = time
            pulse_ADC = pulse/0.1220703125 # convert the pulse voltage (Mv) to ADC unit
            fig, ax1 = plt.subplots()
            ax2 = ax1.twinx()
            ax1.plot(time - time[0], pulse)
            ax2.plot(time - time[0], pulse_ADC)
            ax1.set_xlabel('Time (ns)')
            ax1.set_ylabel('Voltage (mV)')
            ax2.set_ylabel('ADC Units')
            plt.title('Gamma')
```

```
            plt.show()
            print('Pulse max height is ' + str(pulse[index_of_max_height]) + ' mV.')
            print('Pulse max height is ' + str(pulse_ADC[index_of_max_height]) + ' ADC units.')
            print('Time of pulse max height is ' + str(time[index_of_max_height]) + '
nanoseconds.')
        if counter >= num_discriminated_pulses:
            break
```

Fast and slow component fitting to exponential and determine the mean decay time by using python algorithm.

```
import csv
import matplotlib.pyplot as plt
import numpy as np
import pandas as pd
import glob
import scipy.optimize
from scipy.optimize import curve_fit
from decimal import Decimal
path = "./"
all_files = glob.glob(path+"/*.csv")
for file_name in all_files:
    data = pd.read_csv(file_name)
    num_pulses = 50000
    #sample_length = sum(1 for line in open(file)) - 1
    sample_length = sum(1 for line in open(file_name)) - 1
    #data = pd.read_csv(file)
    time_data = data[[f'time{i+1}(ns)' for i in range(50000*0,50000*1)]].to_numpy().T
    pulse_data = data[[f'pulse{i+1}(mV)'for i in range(50000*0,50000*1)]].to_numpy().T
    # *1,2,3,4 … present the order of files
      counter1 = 0
```

```
for pulse,time in zip(pulse_data, time_data):
    index_of_max_height = counter1
    max_height = max(pulse) # To determine the pulse max-height for each time interval
    for i,height in enumerate(pulse):
        if height >= max_height:
            index_of_max_height = i
            break
    if max_height >= 350: # the algorithms only count the max-height was equal to
    350 mV or above it
        counter1 += 1
discriminated_time_data = np.zeros(shape=(counter1, sample_length))
discriminated_pulse_data = np.zeros(shape=(counter1, sample_length)
fast_component = np.zeros(counter1)
slow_component = np.zeros(counter1)
counter2 = 0
for pulse,time in zip(pulse_data, time_data):
    index_of_max_height = counter2
    max_height = max(pulse)
    for i,height in enumerate(pulse):
        if height >= max_height:
            index_of_max_height = i
            break
```

```
            if max_height >= 350:
                discriminated_pulse_data[counter2] = pulse/max_height
        # to convert the y-axis to the normal distribution (using each pulse divided by the
max_pulse)
                discriminated_time_data[counter2] = time-time[index_of_max_height] # make the
time(ns)= 0 for each column
                counter2 += 1
        lambdas_fast = np.zeros(int(len(discriminated_pulse_data)))
        lambdas_slow = np.zeros(int(len(discriminated_pulse_data)))
        def monoExpZeroB(x, m, t): # the name of method to fitting the exponential curve
            return m * np.exp(-t * x)
        for counter1,(pulse,time) in
enumerate(zip(discriminated_pulse_data,discriminated_time_data)):
            height = max(pulse)
            index_of_height = 0
            for counter2,i in enumerate(pulse):
                if i >= height:
                    index_of_height = counter2
            pulse_data_fast = pulse[index_of_height:(index_of_height+5)]
            time_data_fast = time[index_of_height:(index_of_height+5)]
            # for the fast component of BaF2, there were only first five data were considered
             to fitting the exponential curve.
```

```
            pulse_data_slow = pulse[index_of_height+5:index_of_height+95]
            time_data_slow = time[index_of_height+5:index_of_height+95]
           # for the slow component of BaF2, there were 95 data after fast components
            were collected to fitting the exponential curve
            p0_fast = (1, 1.25) # start with values near those we expect
            paramsB_fast, cv_fast = scipy.optimize.curve_fit(monoExpZeroB, time_data_fast,
pulse_data_fast, p0_fast)
            mB_fast, tB_fast = paramsB_fast
            tauSec_fast = (1 / tB_fast)
            #print(f"P_fast = {mB_fast} * e^(-{tB_fast} * t)")
            #print(f'Fast Component={tauSec_fast}')
            total_time_data = np.arange(190)
            PB_fast = monoExpZeroB(total_time_data, mB_fast, tB_fast)
            p0_slow = (0.2, 0.00159) # start with values near those we expect
            paramsB_slow, cv_slow = scipy.optimize.curve_fit(monoExpZeroB, time_data_slow,
pulse_data_slow, p0_slow)
            mB_slow, tB_slow = paramsB_slow
            tauSec_slow = (1 / tB_slow)
            #print(f"P_slow = {mB_slow} * e^(-{tB_slow} * t)")
            #print(f'Slow Component={tauSec_slow}')
            PB_slow = monoExpZeroB(total_time_data, mB_slow, tB_slow)
```

```
fast_component[counter1] = tauSec_fast

slow_component[counter1] = tauSec_slow

plt.plot(time_data_fast, pulse_data_fast, 'o', color='g', label="Fast data")

plt.plot(time_data_slow, pulse_data_slow, 'o', color='b', label="Slow data")

plt.ylim([0,1])

plt.xlim([0, 190])

plt.xlabel('Time (ns)')

plt.ylabel('Normalized Pulse')

plt.title('Fitting Exponential Curve')

plt.legend()

plt.show()

plt.plot(time_data_fast, pulse_data_fast, 'o', color='g', label="Fast data")

plt.plot(total_time_data, PB_fast, '--', color='r', label="Fast data fitted")

plt.ylim([0,1])

plt.xlim([0, 190])

plt.xlabel('Time (ns)')

plt.ylabel('Normalized Pulse')

plt.title('Fitting Exponential Curve')

plt.legend()

plt.show()

plt.plot(time_data_slow, pulse_data_slow, 'o', color='b', label="Slow data")

plt.plot(total_time_data, PB_slow, '--', color='m', label="Slow data fitted")
```

```
plt.ylim([0,1])

plt.xlim([0, 190])

plt.xlabel('Time (ns)')

plt.ylabel('Normalized Pulse')

plt.title('Fitting Exponential Curve')

plt.legend()

plt.show()
```

The algorithm of broadening all the energy bins to Gaussian distribution pulses in MATLAB.

```
clear all

close all

clc

A = load("GammaSpec");

len = length(A);

En(:) = A(:,1);

#read counts column

counts = A(:,2);

#read energy column

R = 0.15;

#Energy Resolution of BaF2 15%=.15, the HPGe energy resolution is 0.3%.

SUM(1:len,1)=0;

for i=1:len

   sigma = R*En(i)/2.35; #calculate the Sigma

   PDF(1:len,1)=0;

   for j = 1:len

      PDF(j,1) = (1/sigma*(sqrt(2*pi)))*exp(-0.5*(((En(j)-En(i))/sigma).^2));
```

```
#calculate the probability density function value
    end
    if i == 1
        SUM(:) = SUM(:) + PDF(:)*counts(i)*En(i)*0.001;
    else
        SUM(:) = SUM(:) + PDF(:)*counts(i)*(En(i)-En(i-1))*0.001;
    end
end
figure(1)
stairs(En(1:len),SUM(1:len));
set(gca,'Yscale','log'); # plot the y-axis as log scale.
xlabel('Energy Deposited (MeV)');
ylabel('counts');
title('BaF2');
grid minor;
grid on;
```